KAOLINITE AND HALLOYSITE DERIVED FROM SEQUENTIAL TRANSFORMATION OF PEDOGENIC SMECTITE AND KAOLINITE-SMECTITE IN A 120 ka TROPICAL SOIL CHRONOSEQUENCE

P. C. Ryan[1,2,*], F. J. Huertas[2], F. W. C. Hobbs[1,3], and L. N. Pincus[1,4]

[1] Geology Department, Middlebury College, Middlebury, Vermont 05753, USA
[2] Instituto Andaluz de Ciencias de la Tierra (CSIC-Universidad de Granada), 18100 Armilla, Granada, Spain
[3] Department of Materials Science and Engineering, University of Wisconsin, Madison, Wisconsin 53706, USA
[4] School of Forestry and Environmental Studies, Yale University, New Haven, Connecticut 06511, USA

Abstract—Tropical soils range from nutrient-depleted lateritic soils rich in halloysite or kaolinite to Inceptisols rich in interstratified kaolinite-smectite (K-S), smectite, or related 2:1 clays. Given the strong influence of clay minerals on tropical soil quality, better understanding of factors influencing their occurrence is important for modeling and managing tropical environments. This study examines the alteration of smectite to kaolinite by way of intermediate K-S and halloysite in a 120 ka moist tropical chronosequence. Iron-rich smectite ($11.6 \pm 2.2\%$ Fe_2O_3) is the dominant mineral in Holocene soils (1−8 ka) originating from sediments rich in plagioclase and clinopyroxene. The cation exchange capacity (CEC) of smectite is 54−84 $cmol_c$/kg and pH is 6.1 to 7.4. Within 50 ka, smectite fixes Al-hydroxy complexes into interlayers, K^+ is retained preferentially over Ca^{2+}, and 2:1 layers are stripped of tetrahedral sheets; the resulting K-S inherits flaky smectite crystal habit and the 2:1 layers − which only expand partially − include Al-hydroxy smectite and some illite-like layers. After 50 ka, the dominant mineral is K-S, the CEC is 18−28 $cmol_c$/kg, and the pH is 5.3. Flaky Fe-kaolinite with ~10% residual smectite layers and halloysite (7.4% Fe_2O_3) also occur in 50 ka soil. The 120 ka soils are dominated by flaky Fe-kaolinite (<10% residual smectite layers) and halloysite (4.9% Fe_2O_3), and Fe-poor hexagonal kaolinite also occurs (5−10% of soil). The CEC is 11−16 $cmol_c$/kg and the pH is 4.7−5.3.

Changes in crystal chemistry of the soil clays (decreasing Fe, Mg, Ca, and K; increasing Al) over time reflects two reaction mechanisms: (1) cell-preserved transformation of smectite layers to kaolinite layers that accompanies conversion of smectite to K-S and eventually kaolinite; this results in the formation of flaky Fe-rich kaolinites after 50 ka; and (2) dissolution of K-S followed by crystallization of halloysite. Neoformation of hexagonal kaolinite and/or halloysite with low Fe (<3% Fe_2O_3) follows dissolution of Fe-kaolinite or halloysite after 100 ka. This sequence is probably common in moist tropical soils and these findings may inform modeling of soil composition in tropical landscapes where tectonic, volcanic, or geomorphic activity periodically exposes unweathered parent material, producing a range of soil ages.

Key Words—Chronosequence, Halloysite, Interstratified, Kaolinite, Smectite, Soil, Soil Age, Tropical.

INTRODUCTION

Understanding the processes and pathways by which soil minerals form is an important component of predicting soil composition but the task becomes complex when considering clay minerals, hydroxides, carbonates, and other pedogenic minerals which experience several generations, or a continuous series, of mineral recrystallization reactions. In the moist tropics, clay minerals are the most abundant solid phase, affecting soil quality more than any other component (Minasny and Hartemink, 2011). In older, well developed, lateritic tropical soils (particularly Oxisols and Ultisols), halloysite and kaolinite are the dominant minerals (Birkeland, 1999). These 1:1 aluminous clays are typically associated with nutrient-poor soils plagued

by small CEC values, significant availability of Al, and a low pH of 4 to 5; note, however, that Oxisols and Ultisols constitute just 43% of soils in the tropics (Szott *et al.*, 1991). Alfisols, many of which are lateritic, make up another 15% (Szott *et al.*, 1991), but the remaining 40% of tropical soils are not leached to a lateritic state; these soils often occur in younger landforms or more poorly drained parts of landscapes (*e.g.* footslopes); they are relatively rich in base cations and Si, favoring the presence of 2:1 clays such as smectite (*e.g.* Ca-K-beidellite), hydroxy-interlayer smectite and vermiculite (HIS and HIV), and interstratified kaolinite-smectite (K-S) (Kantor and Schwertmann, 1974; Delvaux *et al.*, 1989; Righi *et al.*, 1999; Ryan and Huertas, 2009). The

* E-mail address of corresponding author:
pryan@middlebury.edu

2:1 soil clays have CEC values that are typically five to ten times greater than kaolinite and they tend to be associated with relatively nutrient-rich soils (Delvaux *et al.*, 1989, 1992).

The two soil-forming factors most responsible for the variation in clay mineralogy − and hence soil quality − in the moist tropics are time, *i.e.* soil age, and topography (Eswaran *et al.*, 1992). In the absence of localized topographic factors that limit leaching, soil age is the factor with greatest influence on moist tropical soil composition, and when leaching over time depletes Si and base cations, soils will evolve to a kaolinite-rich mineralogy (Nieuwenhuyse *et al.*, 2000); considering these factors, chronosequences provide a useful natural setting to quantify rates of soil evolution. They consist of soils exposed to similar soil-forming factors with one exception, soil age. This means that differences in soil properties of a chronosequence are those that accrue over time. Marine and fluvial terraces, glacial deposits, and volcanic deposits are common chronosequence parent materials (Stevens and Walker, 1970). In many moist tropical soils, smectite forms in the early stages of pedogenesis, often directly from dissolution of primary minerals (Eswaran and DeConinck, 1971; Nahon and Colin, 1982; Singh and Gilkes, 1993). Chronosequence studies indicate that early-stage, smectite-rich brown Inceptisols evolve over time to kaolinite-rich, red lateritic soils (Alexander and Holowaychuk, 1983; Nieuwenhuyse *et al.*, 2000; Kautz and Ryan, 2003; Fisher and Ryan, 2006; He *et al.*, 2008; Ryan and Huertas, 2009). The smectites and related 2:1 clays tend to occur in young tropical soils where limited time is responsible for limited leaching of Si and base cations. These Inceptisols are some of the most productive soils in the tropics (Lal, 1995).

The time span needed to foster alteration from smectite-rich to kaolinite-rich soil in the tropics is on the order of 10^4 to 10^6 y (Tardy and Roquin, 1992; Wilson, 1999; Nieuwenhuyse *et al.*, 2000; Kautz and Ryan, 2003; He *et al.*, 2008; Ryan and Huertas, 2009). A more precise time constraint is limited by insufficient data on soil age or − when soil ages are known − by the lack of soils with intermediate compositions (*i.e.* sequences that contain smectite-rich and kaolinite-rich end members but not intermediate K-S or halloysite). These deficiencies have prevented precise determination of alteration rate (*e.g.* Delvaux *et al.*, 1989; Nieuwenhuyse *et al.*, 2000; Ryan and Huertas, 2009). Improved knowledge of the relationship of soil age to soil composition is required for modeling tropical soils (Jiang *et al.*, 2011), especially in tectonically and volcanically active tropical regions where soils of a given landscape may vary widely in age − examples include large regions of Central and South America, central Africa, southeast Asia, and Hawaii.

Studies documenting of K-S as an intermediate phase in the alteration of smectite to halloysite or kaolinite in tropical soil are relatively few in number (*e.g.* Herbillon *et al.*, 1981; Alexander and Holowaychuk, 1983; Yerima *et al.*, 1985; Delvaux *et al.*, 1989; Bühmann and Grubb, 1991; Delvaux and Herbillon, 1995; Nieuwenhuyse *et al.*, 2000; Ryan and Huertas, 2009). One possible explanation for the paucity of documented occurrences of the smectite → K-S → halloysite and/or kaolinite sequence is that K-S is difficult to identify in routine analyses; it is easy to misinterpret as end-member smectite in cases of smectite-rich K-S, or as halloysite or disordered kaolinite in cases of kaolinite-rich K−S (Hughes *et al.*, 1993; Cuadros *et al.*, 1994; Delvaux and Herbillon, 1995; Środoń, 1999). Recognition of K-S is important because it has a greater CEC than kaolinite and, as a precursor phase, can influence the composition (and hence reactivity) of later-stage halloysite or kaolinite (Ryan and Huertas, 2013).

In spite of decades of research (*e.g.* Brindley, 1961; Keller, 1977; Bailey, 1989; Churchman and Gilkes, 1989; Petit and Decarreau, 1990; Ndayiragije and Delvaux, 2003), the relationship of halloysite or kaolinite to each other, or to precursor clays, is still not fully understood (Hart *et al.*, 2002; Hughes *et al.*, 2009). Thermodynamic data indicate that kaolinite is stable relative to halloysite (Dean, 1979; de Ligny and Navrotsky 1999; Fritz *et al.*, 2009) and the expected alteration of halloysite to kaolinite has been observed in soil (Parham, 1969; Eswaran and Wong, 1978; Calvert *et al.*, 1980; Churchman and Gilkes, 1989; Delvaux *et al.*, 1992; Abayneh *et al.*, 2006). Interestingly, the reverse has also been observed, seemingly as a result of the hydration of kaolinite which causes rolling of 1:1 layers (Robertson and Eggleton, 1991; Singh and Gilkes, 1992; de Oliveira *et al.*, 1997). Halloysite and kaolinite can also crystallize in soil from precursor smectite by way of interstratified K-S or halloysite-smectite (H-S) (Wada and Kakuto, 1983; Karathanasis and Hajek, 1984; Delvaux *et al.*, 1989; Ryan and Huertas, 2009), seemingly on a path toward thermodynamic stability. Halloysite and kaolinite may also precipitate directly from solution or from products of primary mineral dissolution (*e.g.* Balan *et al.*, 2007; Etame *et al.*, 2009; Berthonneau *et al.*, 2015).

The range of explanations for the origins of tropical soil mineral assemblages led Hart *et al.* (2002) to indicate that no coherent model exists to explain the variability observed in composition or morphology of halloysites and kaolinites in tropical soils. Yet the smectite → K-S (or H-S) → halloysite and/or kaolinite reaction sequence has been documented in the tropics of Africa (Kantor and Schwertman, 1974; Herbillon *et al.*, 1981; Delvaux *et al.*, 1990b), Central and South America (Alexander and Holowaychuk, 1983; Yerima *et al.*, 1985; Ryan and Huertas, 2009), and southeast Asia (Jiang *et al.*, 2011), suggesting that the systematic evolution over time from 2:1 to 1:1 clays by way of intermediate phases may be more common than

currently recognized. Given the strong influence of soil clays on tropical soil quality (Misasny and Hartemink, 2011), the recognition and application of such a paradigm could prove significant.

Understanding the origin of Fe in halloysite and kaolinite is important because it influences the structure and reactivity of these clays. A greater amount of octahedral Fe results in disordered kaolinites with 1:1-layer stacking faults, greater surface area, and greater surface charge compared to well-crystallized, low-Fe kaolinites (Balan et al., 1999; Wilson, 1999; Hart et al., 2002; Hughes et al., 2009). Like soil kaolinites, soil halloysites also exhibit a range of composition, e.g. from very low-Fe (<0.5% Fe_2O_3) to very high-Fe specimens (up to 12.8% Fe_2O_3; Herbillon et al., 1976; Wada and Mizota, 1982), with CEC that correspondingly ranges from 5 to 50 $cmol_c/kg$ (Grim, 1968; Ma and Eggleton, 1999; Joussein et al., 2005; Pochet et al., 2007). One possible explanation for the range of Fe in 1:1 soil clays is inheritance from precursor smectite or K-S (Ryan and Huertas, 2013), emphasizing the importance of characterizing the smectite to halloysite or kaolinite reaction sequence.

Given the strong influence of time on the mineralogical and chemical composition of tropical soil (Eswaran et al., 1992; Nieuwenhuyse et al., 2000; Gracheva et al., 2001; Fisher and Ryan, 2006), improved knowledge of the sequential stages that occur as a function of soil age should prove valuable when trying to predict or model soil quality (provided that soil age is known or can be inferred). Two recent reports on tropical soils (Uehara, 2003; Minasny and Hartemink, 2011) address the need for research on tropical soil composition, indicating that with mineralogical and chemical analysis, attributes of tropical soils (e.g. ion-exchange capacity, potential for adsorption-desorption, soil-aggregate formation, hydraulic conductivity, gas transport) can be predicted. Such analyses are not commonly performed when soil surveys are conducted; for this reason, mineralogical and compositional research that facilitates modeling of soil attributes is needed, especially in the tropics where "the dearth of soil property measurements is large" (Minasny and Hartemink, 2011).

An opportunity to examine temporal relationships of pedogenic clay minerals is provided by a dated tropical chronosequence in northwestern Costa Rica. The soils are Inceptisols and lateritic Alfisols that range in age from 1 to 120 ka and have formed by weathering of terrace sediments for which soil-forming factors other than time (i.e. soil age) are similar. Previous studies in this region indicate that, in Holocene terrace soils, smectite is the dominant early pedogenic mineral (Fisher and Ryan, 2006; Hobbs, 2012); smectite is then altered to halloysite and kaolinite over time by way of interstratified K-S (Ryan and Huertas, 2009). The series of reactions is driven by leaching of base cations and Si, and the rates and mechanisms associated with develop-

ment of the halloysite+kaolinite assemblage are important to characterize because this assemblage represents an effective steady state in lateritic soils achieved after 10^4-10^6 y of pedogenesis (Askenasy et al., 1973; Bravard and Righi, 1988; Schaefer et al., 1988; Tardy and Roquin, 1992; Nieuwenhuyse et al., 2000; Kautz and Ryan, 2003; Ryan and Huertas, 2009; Silva et al., 2013). Given this background, the well-dated terrace chronosequence on the southern Nicoya Peninsula of Costa Rica (Marshall and Anderson, 1995; Sak et al., 2009; Hobbs, 2012; Marshall et al., 2012) provides an excellent opportunity to examine the reaction rate and the effect of time (soil maturation) on the origin, occurrence, morphology, alteration mechanisms, crystal chemistry, and mineralogical structures of pedogenic smectite, K-S, halloysite, and kaolinite. The main hypothesis is that the Nicoya chronosequence soils will exhibit systematic evolution over time from smectite-dominated to kaolinite-dominated by way of intermediate minerals (K-S, halloysite, and Fe-kaolinite with residual interstratified smectite), and that the soil ages and mineralogical data provided by this chronosequence will help to constrain rates and mechanisms of alteration associated with the progression to a halloysite+kaolinite-dominated mineral assemblage.

CHRONOSEQUENCE DESCRIPTION

Marine terraces on the Nicoya Peninsula of northwestern Costa Rica (Figures 1, 2; Table 1) have been created by uplift associated with convergence of the Cocos Ridge (a bathymetric high in the oceanic Cocos Plate) and the Caribbean Plate (Marshall and Anderson, 1995). Soils developed on the terraces are derived from sandy and pebbly beach and shallow-marine parent material that is a combination of andesitic-basaltic volcaniclastic detritus, material eroded from marine sedimentary and mafic rocks of the Nicoya Complex (Lundberg, 1991), and shell fragments.

Holocene (≤8 ka) terrace soils termed Qt4 and Qt3 occur at low elevations (<40 m above mean sea level, m.a.s.l.); they are dark brown, gray, and black Lithic Ustorthents and Lithic Ustropepts rich in organic matter and primary minerals including plagioclase, clinopyroxene, and quartz, with accessory heulandite, volcanic ash, and calcite (in shell fragments) (Hobbs, 2012). The lowest-elevation soils (<5 m.a.s.l.) have a water table located 50 to 100 cm below land surface (when sampled during the rainy season in late August) − this was the case for Qt4, but the older Holocene soils (Qt3) showed no evidence of water table to a depth of at least 1 m. Soils developed on Pleistocene terraces (~60−250 m.a.s.l.; referred to as Qt2 and Qt1) are lateritic in appearance, have little visible organic matter, and are classified mainly as Ustic Dystropepts and Ultic Haplustalfs. These soils show no evidence of water table to a depth of at least 3 m and are well drained. The soil
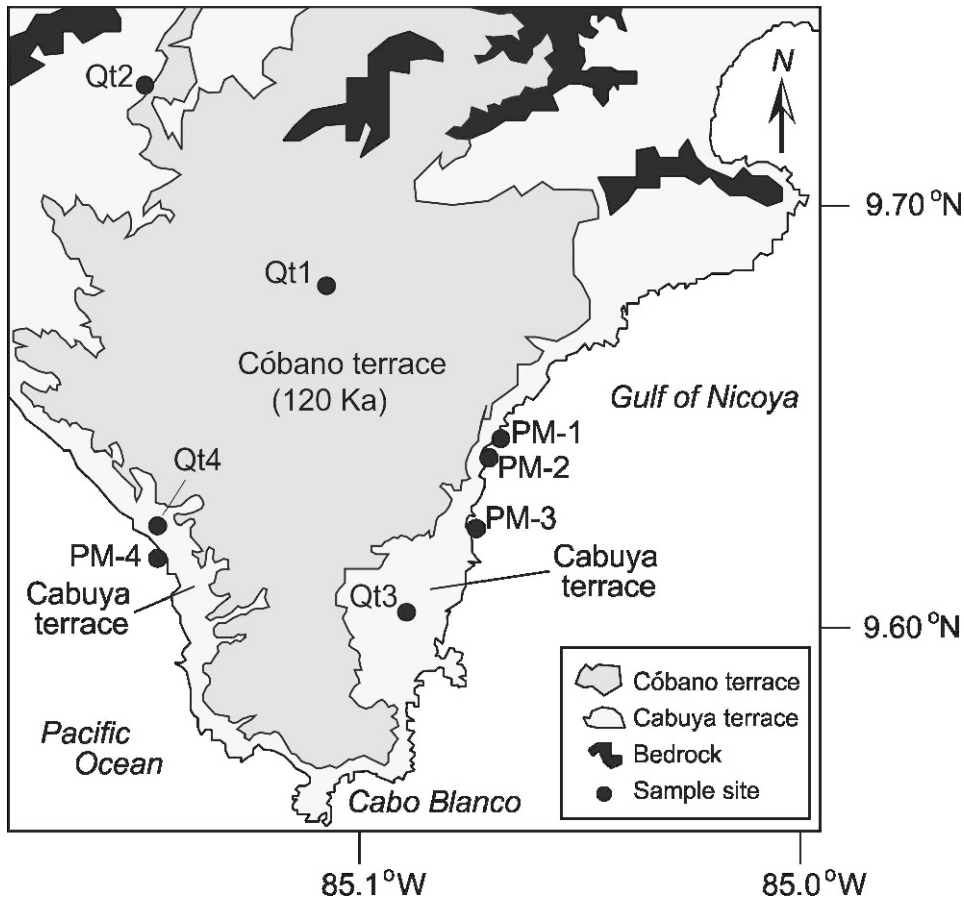
Figure 1. Location map of the study area at the southern tip of Nicoya Peninsula, Costa Rica. The main marine terrace sets are: (1) the near-shore, low-elevation Holocene (1−8 ka) Cabuya terrace group (Qt4, Qt3); (2) the higher-elevation Pleistocene (120 ka) Cóbano terrace (Qt1); and (3) intermediate-aged terraces preserved locally between the Cabuya and Cóbano terraces (*e.g.* Qt2, a 50 ka terrace in the northwestern part of the study area). Ages are based on radiocarbon and OSL dates from Sak *et al.* (2009), Marshall *et al.* (2007, 2012), and Hobbs (2012).

taxonomy information listed here was produced by the Oficina de Planificación Sectorial Agropecuaria, San José, Costa Rica, in 1978 and made available on-line as 1:200,000 maps by Selvaradjou *et al.* (2005).
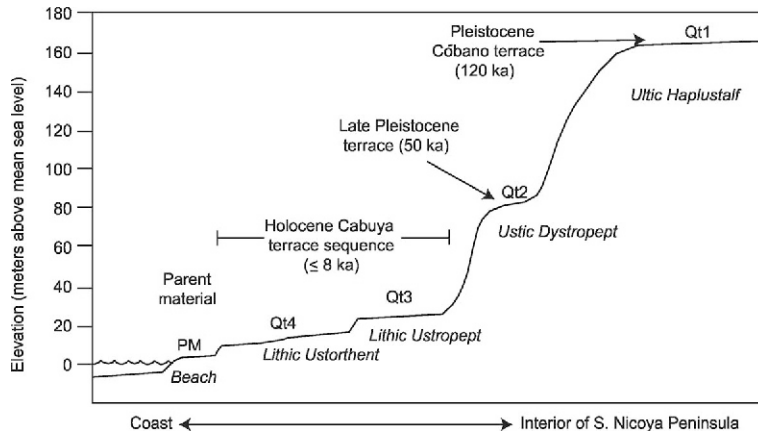

Figure 2. Schematic sketch of the Nicoya chronosequence showing the elevational relationship of sampled materials, from parent material (beach sand) to soils formed on uplifted Holocene and Pleistocene terraces. Terrace IDs are shown (Qt1−Qt4).

Table 1. Sample IDs, descriptions, ages, surface elevations, latitude and longitude information for sample sites, depth of sampled material (below land surface, cm), and, for soils, Munsell color data, CEC, and pH. Ages are terrace depositional ages.

Sample ID	Type	Age (ka)	Elev (masl)	LAT	LONG	Depth	Color	CEC	pH
PM-1	Beach sediment	0	1	9.64435	85.0728	20	tan and black	–	–
PM-2	Beach sediment	0	1	9.64435	85.0728	20	sand with peb-	–	–
PM-3	Beach sediment	0	1	9.62233	85.0791	20	ble-sized shell	–	–
PM-3	Beach sediment	0	1	9.62783	85.1505	20	clasts	–	–
Qt4 (20 cm)	Holocene terrace AB horizon	2	10	9.62632	85.1513	20	2.5Y 3/1	83.7	7.4
Qt3 (20 cm)	Holocene terrace AB horizon	8	30	9.60528	85.0942	20	7.5YR 4/1	53.9	6.1
Qt2 (20 cm)	Pleistocene terrace B1 horizon	50	80	9.73302	85.1536	20	5YR 4/6	20.5	5.3
Qt2 (50 cm)	Pleistocene terrace B2 horizon		80	9.73302	85.1536	50	5YR 4/6	18.0	5.1
Qt2 (150 cm)	Pleistocene terrace C horizon		80	9.73302	85.1536	150	10YR 5/6	27.7	5.3
Qt1 (20 cm)	Pleistocene terrace B1 horizon	120	170	9.68477	85.1105	20	10R 3/6	16.4	5.3
Qt1 (50 cm)	Pleistocene terrace B2 horizon		170	9.68477	85.1105	50	10R 4/4	11.3	4.9
Qt1 (100 cm)	Pleistocene terrace B3 horizon		170	9.68477	85.1105	100	10R 4/4	11.4	5.1
Qt1 (300 cm)	Pleistocene terrace deep B horizon		170	9.68477	85.1105	300	2.5YR 4/6	11.6	4.7

In an idealized chronosequence, all soil-forming factors except soil age are constant, allowing researchers to examine rates of soil formation and evolution (Stevens and Walker, 1970). In the sequence studied herein, time (120 ka) is the factor with the greatest influence on soil composition. Regarding the other soil-forming factors: (1) climate is virtually identical for all sites sampled; during cooler parts of the Pleistocene, however, mean annual precipitation (MAP) was probably less than the current 2800−3200 mm and the mean annual temperature was probably 3 to 5ºC less than the current 27ºC (Greene et al., 2002); (2) dry tropical forest occupies much of the Nicoya Peninsula, although drier conditions during cooler Pleistocene periods might have led to a more savanna-like ecosystem during the last glacial maximum at 21 ka (Piperno and Jones, 2003); (3) the terraces are relatively flat and only locally dissected, and the only appreciable occurrences of poorly drained soils in the southern Nicoya Peninsula are found in young terraces at low elevations (≤ 5 m.a.s.l.), where poor drainage is caused by abundant smectite which lowers hydraulic conductivity, and low slope of the water table which causes slow flow. The interrelated smectite-rich/low topographic elevation/poor drainage factors are a function of time, and these attributes are only associated with the youngest soils in this sequence; (4) parent material (beach sediment) collected from the perimeter of the field area is compositionally similar, i.e. is mainly andesitic basalt and mixed sedimentary detritus with similar Zr:Ti

ratios (see below) across location and time (Lundberg, 1991; Hobbs, 2012). The main exception to this is varied $CaCO_3$ due to shelly fossils mainly in the silt and coarser fractions. Overall, the main factor controlling the differences in soil mineralogy of this coastal landscape is time; this study, therefore, is concerned with analysis of temporal controls on tropical soil mineralogy and the implications of this relationship (soil age and composition) for tropical landscapes.

The age of a given terrace (Table 1) represents emergence above sea level corresponding to onset of subaerial soil formation (Anderson et al., 1999). The 2 ka age of Qt4 is based on 16 radiocarbon dates of shells and beachrock in Qt4 soils that fall between 1.1 and 2.8 ka (Sak et al., 2009; Hobbs, 2012). The 8 ka age for the Qt3 Holocene terrace is based on: (1) a calculated age given current Qt3 elevation of 30 m and an uplift rate of 3 to 5 m/ka (Sak et al. 2009), values which indicate exposure of the subaerial terrace between 6 and 10 ka; (2) the constraint of sea level rise, which by 8 ka had slowed sufficiently to a rate less than uplift rate, meaning terraces could form; and (3) geographic proximity to, and geomorphic location above, radio-carbon-dated 5−7 ka terraces (Sak et al., 2009). The 50 ka age for Qt2 is based on a calibrated 48 ka radiocarbon date (accelerator mass spectrometer) of marine shells sampled from this terrace, and it has been correlated to the marine isotope stage 3 sea level high stand at 50 ka (Marshall et al., 2007). The 120 ka age for Qt1 is based on a 111 ka optically stimulated

luminescence (OSL) date that has been correlated to the 120 ka marine isotope stage 5e high stand (Marshall *et al.*, 2012).

Mean annual precipitation in the 70 km^2 study area of the southern Nicoya Peninsula is 2800–3200 mm/y and the mean annual temperature is 27ºC; precipitation is seasonal, characterized by a 5-month dry season (December−May) during which <100 mm of rain falls (Instituto Meteorológico Nacional of Costa Rica; Albertin, 1962). This area is defined as a tropical rainy climate with winter dry season ("Aw" in the Köppen system and "dry tropical forest" in the Holdridge system). In this paper the term "moist tropics" is based on the Köppen system (Af, Am, Aw) to represent areas with annual rainfall of >500 mm/y, which generally coincides with sufficient infiltration and leaching to favor formation of halloysite or kaolinite given enough time. In this study area, ~50% of forest has been cleared for agriculture, mostly grazing.

MATERIALS AND METHODS

Sampling strategy

Holocene soil samples were obtained by digging 0.5 to 1 m down into terrace soils, and Pleistocene terrace soils were sampled from recently exposed road cuts, in some cases to a depth of 3 m below terrace surface (Hobbs, 2012). When sampling roadcuts, 50 cm of soil overburden was removed to ensure that samples were of fresh soil. Samples were double-bagged to preserve field moisture. Initially, 62 soil samples constituting horizons from 13 locations were analyzed by X-ray diffraction (XRD) of <2 µm fractions on oriented slides for mineralogical content (Hobbs, 2012). From this initial suite, 27 horizons that were representative of the sequence were selected for inductively coupled plasma-atomic emission spectrometry (ICP-AES) and XRD analysis of <2 mm powders at Middlebury College, Vermont, USA (Hobbs, 2012). From that suite, nine soil horizons (Table 1) which are representative of the clay-mineral alteration sequence were selected for additional analysis by detailed XRD, transmission electron microscopy (TEM), and Fourier-transform infrared (FTIR) spectroscopy. These nine samples included smectite-rich and kaolinite-rich end-members as well as intermediate stages (K-S, halloysite, and flaky Fe-kaolinite). Details of analytical methods follow.

Bulk-soil chemistry

Approximately 20 g of well-mixed soil was separated for chemical and mineralogical analysis of the bulk (<2 mm) fraction. These samples were dried at 60ºC, ground gently to disaggregate, and then sieved to collect the <2 mm fraction. The chemical composition of this fraction was determined by ICP-AES using a Thermo Jarrell Ash Iris 1000 (Waltham, Massachusetts, USA) at Middlebury College. The <2 mm samples were dried at

100ºC to drive off adsorbed water, and loss on ignition (LOI) was determined at 1050ºC followed by fusion with a flux powder at 1050ºC (flux powder: ultra pure 50% lithium metaborate − 50% lithium tetraborate from Spex, Metuchen, New Jersey, USA). Fused samples were dissolved in 5% HNO$_3$ (trace-metal grade, Fisher Scientific) to produce the solution for analysis by ICP-AES. Analyses of the US Geological Survey basalt standard MRG-1, US Geological Survey andesite standard AGV-2, and replicate analyses of unknowns indicated that uncertainties were ±3% for major elements except K$_2$O and MgO, for which uncertainties were ±5%. Uncertainties for trace elements were ±5% (except for concentrations <100 ppm, where uncertainty approached 10%).

Uniformity of parent material was assessed geochemically using the ratio of ZrO$_2$:TiO$_2$ (Reheis, 1987) as well as by assessing similarity of grain size and chemical and mineralogical constituents present in beach sand parent material from sites adjacent to sampled Holocene soils.

Soil pH and CEC

Soil pH was determined by the 2:1 (water:soil) method (Thomas, 1996) by mixing 10 mL of deionized water (MilliQ) with 5 g of soil (<2 mm fraction). After sonification and gravity settling, the pH values were recorded on an Oakton pH 700 meter calibrated with pH 4.01, 7.00, and 10.00 buffered solutions. The precision of results was 0.1 units of pH.

Cation exchange capacity (CEC) of the clay fraction was determined by ammonium acetate extraction (Madeira *et al.*, 2003; Navarrete *et al.*, 2009), as follows. Subsamples (2.5 g) of the dried <2 µm fraction were weighed into a 100 mL beaker with 50 mL of 1 M NH$_4$OAc at pH 7 (reagent grade NH$_4$OAc, Sigma Aldrich, Germany). Details of the extraction process were given by Pincus (2014). Following extraction, solutions were analyzed using the Thermo Jarrell Ash IRIS 1000 spectrometer (described above). Data output (mg/L) was converted to cmol$_c$/kg to determine individual cation contributions to CEC. Concentrations of Ca, K, Na, and Mg were summed to determine total CEC of the soil clays (Pincus, 2014). Uncertainty/error was determined by running blanks and replicates, and by comparison of experimental with published values. For the smectites Mont-20 and STx-1B (Harward *et al.*, 1969; Shainberg *et al.*, 1987; Borden and Giese, 2001), % error (uncertainty) was 10%, *e.g.* 100 ± 10 cmol$_c$/kg. For standards with CEC values ⩽20 cmolc/kg (*e.g.* Hall-12, KGa-2, PFl-1; Black, 1965; Borden and Giese, 2001), error estimates were 50% of published values, *e.g.* 12 ± 6 cmol$_c$/kg.

Mineralogy

Bulk soil mineralogy (<2 mm) was determined by XRD analysis of random powders containing 10% ZnO

(as an internal standard) which were micronized prior to side-loading (Hobbs, 2012). Oriented powders were prepared from field-moist soils by first isolating the <2 μm fraction by settling in cylinders then by pipetting concentrated suspensions of ~100 mg clay onto glass slides. These preparations were scanned continuously from 3 to 40º2θ (3.5º/min) in air-dried (AD), ethylene glycol-solvated (EG, analytical grade, Probus, Badalona, Spain), and sequentially heated states (350ºC for 1 h, then 550ºC for 2 h). The XRD analyses presented here were performed using a PANalytical X'Pert Pro system (Almelo, The Netherlands) at the Instituto Andaluz de Ciencias de la Tierra (IACT), operating with a θ−θ goniometer at 45 kV and 40 mA with an X'Celerator detector, CuKα radiation, Ni filter, and divergence and anti-scatter slits of 1/4 and 1/2º, respectively. Analyses were performed on Ca-saturated specimens.

The percentage of kaolinite in interstratified K-S was calculated by comparing experimental XRD patterns of oriented slides with calculated patterns produced using *NEWMOD* (Reynolds, 2012) and with data in Cradwick and Wilson (1972) and Moore and Reynolds (1997), with an estimated uncertainty of ±10% in the range 60−90% K (in K-S) and ±5% in the range 90−100% K in K-S. Percent kaolinite layers in K-S was also constrained by TEM-AEM (see below) and this was also taken into account in error quantification.

Random powder mounts of the <2 μm fraction were analyzed to determine mean *b*-axis dimensions of 2:1 and 1:1 layers – these were prepared from <2 μm fractions of Ca-saturated powders (scraped off oriented slides and ground gently) that were sprinkled onto a zero-background silicon sample holder, cut with a razor blade to enhance the intensity of *hkl* peaks, and coalesced using analytical-grade acetone (Merck, Darmstadt, Germany). These preparations were analyzed from 3 to 70º2θ (1.5º/min) and then, to enhance analysis of the 06,33 region of the clay minerals, from 58−65º2θ (0.5º/min).

Single-crystal chemistry

The textures and compositions of single crystals were analyzed by transmission electron microscopy paired with analytical electron microscopy (TEM-AEM) at the Centro de Instrumentación Científica (CIC) in Granada, Spain, using a Philips CM-20 instrument (Almelo, The Netherlands) fitted with an ultrathin window and solid-state Si(Li) detector for energy dispersive X-ray analysis (EDAX©; Mahwah, New Jersey, USA). The Ca-saturated <2 μm fraction of each specimen was suspended in pure ethyl alcohol and mounted on Cu grids, then analyses were performed at 200 kV with a 70 nm spot size and a point-to-point resolution of 2.7 Å in TEM mode. Atomic proportions calculated from EDAX peak intensities were converted to atomic concentrations using a variety of natural mineral standards, and quantitative calibration was carried out

by the method of Cliff and Lorimer (1975). Transmission electron microscopy-analytical emission microscopy cannot distinguish ferric from ferrous iron, so, given the predominantly oxidizing conditions in these soils, and Mössbauer and X-ray absorption spectroscopy evidence for the prevalence of octahedral Fe^{3+} over Fe^{2+} in soil-formed Fe-smectites (*e.g.* Gaudin *et al.*, 2004), all iron was cast here as Fe^{3+}. The percentage of kaolinite layers in interstratified K-S was estimated by extrapolation from smectite and kaolinite end-member compositions. Variability in end-member composition (especially smectites) produced an uncertainty of ~±10% except where % kaolinite in K-S is >90% (*i.e.* error estimates were, *e.g.* 70 ± 10% or 90 ± 5% K in K-S). Contamination from non-target minerals was minimal; *e.g.* nanometer-scale Fe-(oxyhydr)oxide growths were observed on some clay crystals, but in cases where contamination was a possibility, compositions were not obtained from these crystals.

Some very thin crystals of kaolinite and K-S in the most-evolved soil samples (Qt1) rapidly lost Al by volatilization during analysis in the TEM-AEM. In order to correct for Al loss (Cuadros *et al.*, 2009), compositions were measured after 15 and 50 s of analysis. Initial Al:Si ratios were calculated by extrapolating to $t = 0$ s and concentrations of Al were determined by multiplying the Al:Si ratio at $t = 0$ by the $t = 50$ s Si value. The Mg, Fe, and Si, which showed no variation during analysis, were obtained from the $t = 50$ s analyses.

To image layer spacings of clay minerals, oriented <2 μm fractions were embedded in epoxy resin and sliced parallel to the *c** axis by an ultramicrotome (Reichert Jung, Vienna, Austria), coated with a carbon film, then analyzed with high resolution TEM (HRTEM) using an FEI Titan G2 60-300 microscope (Eindhoven, The Netherlands) at CIC in Granada, Spain, with an extra-high brightness field emission gun (XFEG), spherical aberration corrector, and HAADF (high-angle annular dark-field imaging) detector, working at 300 kV, with a resolution of 0.8 Å in the TEM mode and 2 Å in the scanning transmission electron microscope (STEM) mode. Energy dispersive X-ray analysis was also performed to produce element maps of single crystals.

Fourier-transform infrared spectroscopy

Information on structure and composition of the clay fraction was obtained from FTIR spectra recorded using a Perkin-Elmer Spectrum One spectrometer (Waltham, Massachusetts, USA) at the IACT in Granada, Spain, in absorbance mode (4000−400 cm^{-1} range) with a resolution of 4 cm^{-1}. Samples were prepared as pressed pellets after mixing 1 mg of sample in 150 mg of dried, spectroscopy-grade KBr (Merck, Darmstadt, Germany). The pellets were heated overnight at 120ºC before analysis.

RESULTS

Information obtained from each of the analytical methods is presented below, and for each method, data from the youngest soils (Qt4 and Qt3) are presented first followed by intermediate age (Qt2), then the oldest soils (Qt1).

Bulk-soil composition

Chemical weathering of uplifted shallow marine sediments results in depletion of soluble constituents (*e.g.* Ca, Na, Mg, K, Si, Sr), leading to increased concentration of residual Al, Fe, and Ti as well as the trace elements Cr, Cu, Ni, V, Zn, and Zr (Table 2). Elemental compositions (especially ratios) of beach sand parent material (PM) are similar among the four PM sites sampled with the exception of Ca, which is influenced by differing abundances of $CaCO_3$-rich shell fragments. The legacy of shell-derived Ca persists into Qt4 (*i.e.* for ~2 ka), after which remaining Ca in the upper 1 m of soil is accounted for by small amounts of as yet, unweathered plagioclase and by Ca in smectite interlayers (see below).

The relatively small variations in the ZrO_2:TiO_2 ratio of beach sand PM (96.4 ± 29) and soils (94.1 ± 24) suggest similarity in terrace-soil parent material (after Reheis, 1987); overall, ZrO_2:TiO_2 is consistent with PM of andesitic-basaltic composition. For comparison, a suite of locally derived volcaniclastic andesitic-basaltic sedimentary rock from Sámara (on the Nicoya Peninsula 60 km northwest of the study area) has a ZrO_2:TiO_2 ratio of 131 ± 35 (Patino *et al.*, 2004), basalt from Nicoya complex basement rock has a ZrO_2:TiO_2 ratio of 84.8 ± 8 (Geldmacher *et al.*, 2008), and basaltic andesite from Rincon de la Vieja volcano (120 km north of the study area) has a mean ZrO_2:TiO_2 of 78 (Szymanski *et al.*, 2013). Thus, three likely sources of sediment PM have ZrO_2:TiO_2 ratios of 78 to 131, very similar to Nicoya parent material and soil (Table 2). For reference, US Geological Survey standard granite (G-2) and granodiorite (GSP-2) have ZrO_2:TiO_2 ratios of 870 and 1126, respectively; USGS standard andesite (AGV-2) has ZrO_2:TiO_2 of 296, and a USGS basalt standard from Iceland (BIR-1) has ZrO_2:TiO_2 of 25. Much of the variability in other major and trace elements is related to varied abundances of $CaCO_3$ from shell fragments. Ratios of elements other than Ca are similar for each PM sample, and when $CaCO_3$ is factored out (by assuming that shelly $CaCO_3$ is all but 2% of CaO in PM), compositional ranges are relatively small for the most abundant elements, *e.g.* SiO_2 (58−65%), Al_2O_3 (13−16%), and Fe_2O_3 (6−10%). Greater PM variability is notable in MgO (3−8%) and K_2O (0.8−2.6%).

Soil pH and CEC

Holocene soil pH values are 7.4 and 6.1 (Qt4 and Qt3). Pleistocene Qt2 (50 ka) soils have pH ranging from

Table 2. ICP-AES data for bulk (<2 mm) beach sand parent material (PM) and for terrace-soil samples (wt.% for major elements, ppm for trace elements). Ages (ka) are depositional ages of terrace sediment. Depth is cm below soil surface. High % CaO in PM is due to shell fragments. (Al+Fe)/bases is $(Al_2O_3+Fe_2O_3)/(MgO+CaO+Na_2O+K_2O)$. All values are presented on an anhydrous basis.

Sample ID	Type	Age	Depth (cm)	SiO_2	TiO_2	Al_2O_3	Fe_2O_3	MnO	MgO	CaO	Na_2O	K_2O	P_2O5	Total	(Al+Fe)/ bases	Cr	Ni	Cu	Sr	V	Zn	Zr	ZrO_2/ TiO_2
PM1	Beach	0	20	32.1	0.44	6.84	4.52	0.09	3.50	49.8	2.28	0.41	0.07	100	0.20	101	63.8	263	1638	114	81.7	19.0	58.2
PM2	Beach	0	20	37.8	0.70	9.36	6.82	0.13	5.30	36.5	2.75	0.53	0.10	100	0.36	154	76.2	64.0	1260	180	93.8	47.6	91.9
PM8	Beach	0	20	52.7	0.71	11.0	6.38	0.17	3.37	21.2	2.34	2.08	0.14	100	0.60	93.9	57.2	81.0	560	134	143	65.4	124
PM20	Beach	0	20	37.4	0.62	9.24	3.19	0.10	1.51	44.8	2.25	0.58	0.27	100	0.25	62.7	13.5	31.1	2020	62.0	84.4	51.0	111
Qt4	Terrace	2	20	57.1	3.47	13.2	13.6	0.15	2.92	6.30	1.64	1.29	0.31	100	2.2	207	53.7	79.3	416	349	118	218	85.0
Qt3	Terrace	8	20	61.3	1.13	16.6	9.89	0.26	4.12	2.35	1.28	2.83	0.19	100	2.5	139	100	152	287	221	185	128	153
Qt2-20	Terrace	50	20	50.5	3.06	21.7	22.3	0.07	1.44	0.42	0.04	0.42	0.06	100	19.0	230	132	180	35.1	686	99.6	210	92.6
Qt2-50	Terrace		50	53.3	3.20	20.9	19.5	0.11	1.71	0.65	0.05	0.52	0.04	100	13.8	200	122	170	36.1	688	239	206	86.8
Qt2-150	Terrace		150	57.6	2.88	20.4	16.2	0.04	2.01	0.30	0.05	0.50	0.03	100	12.8	235	102	158	22.0	642	154	196	92.1
Qt1-20	Terrace	120	20	42.4	2.00	31.3	22.6	0.23	0.81	0.47	0.05	0.03	0.06	100	39.4	434	275	285	53.0	416	185	118	79.9
Qt1-50	Terrace		50	43.9	2.08	29.6	22.6	0.36	0.77	0.48	0.05	0.07	0.05	100	38.0	464	236	258	47.9	462	218	133	86.7
Qt1-100	Terrace		100	43.4	2.19	30.2	22.6	0.29	0.79	0.40	0.05	0.06	0.05	100	40.5	383	230	237	46.3	474	154	166	102
Qt1-300	Terrace		300	43.1	1.97	31.0	22.2	0.29	0.96	0.29	0.05	0.11	0.04	100	38.0	478	458	404	62.0	390	112	101	69.4

5.1 to 5.3 and Qt1 soils have pH ranging from 4.7 to 5.3 (Table 1). These values and the trend of decreasing pH with age are similar to what was observed 80 km to the southeast in a chronosequence in slightly moister soils (Fisher and Ryan, 2006).

The CEC of the clay fraction of Qt4 soil (2 ka) was 83.7 $cmol_c$/kg while Qt3 (8 ka) had a value of 53.9 $cmol_c$/kg. In 50 ka Qt2, CEC varies with depth from 20.5 $cmol_c$/kg in the B1 horizon (20 cm depth) to 18.0 $cmol_c$/kg in B2 (50 cm) and 27.7 $cmol_c$/kg at a soil depth of 150 cm. The clay fraction of the oldest soils (Qt1, 120 ka) had CEC values of 16.3 $cmol_c$/kg in the B1 (20 cm) and 11.3 to 11.6 $cmol_c$/kg in deeper horizons (Table 1). The presence of small amounts (<5%) of calcite and heulandite in Qt4 could have released Ca or other base cations, resulting in an apparent CEC that is greater than that due to smectite alone (Dohrmann, 2006). The measurements also do not include exchangeable Al or H^+.

Soil mineralogy − XRD

Qt4 and Qt3. Random powder XRD analysis (Figure 3) of the <2 μm fraction of both the 2 ka (Qt4) and 8 ka (Qt3) soils indicated that smectite is the dominant mineral, with a 001 peak at 13−14 Å (air-dried) and a 02,11 band with a peak maximum at ~4.49 Å that tails off toward higher *d* values with no observable *hkl* peaks. The 06,33 region contains a broad 1.504 Å peak (Figure 3b), consistent with a smectite *b*-axis dimension of 9.02 Å. Quartz is present in both Qt4 and Qt3, and the presence of a small amount of calcite (remnants of shell fragments visible in hand sample) in Qt4 is indicated by the weak but sharp peak at 3.04 Å (29.4º2θ). The presence of a small amount of heulandite in Qt4 is indicated by the peak at 8.94 Å (9.9º2θ) and a small amount of mica in Qt3 is indicated by the weak, sharp 001 peak at 10 Å (8.8º2θ).

Oriented XRD mounts of the <2 μm fraction (Figure 4a) indicate that smectite in Qt4 produces a
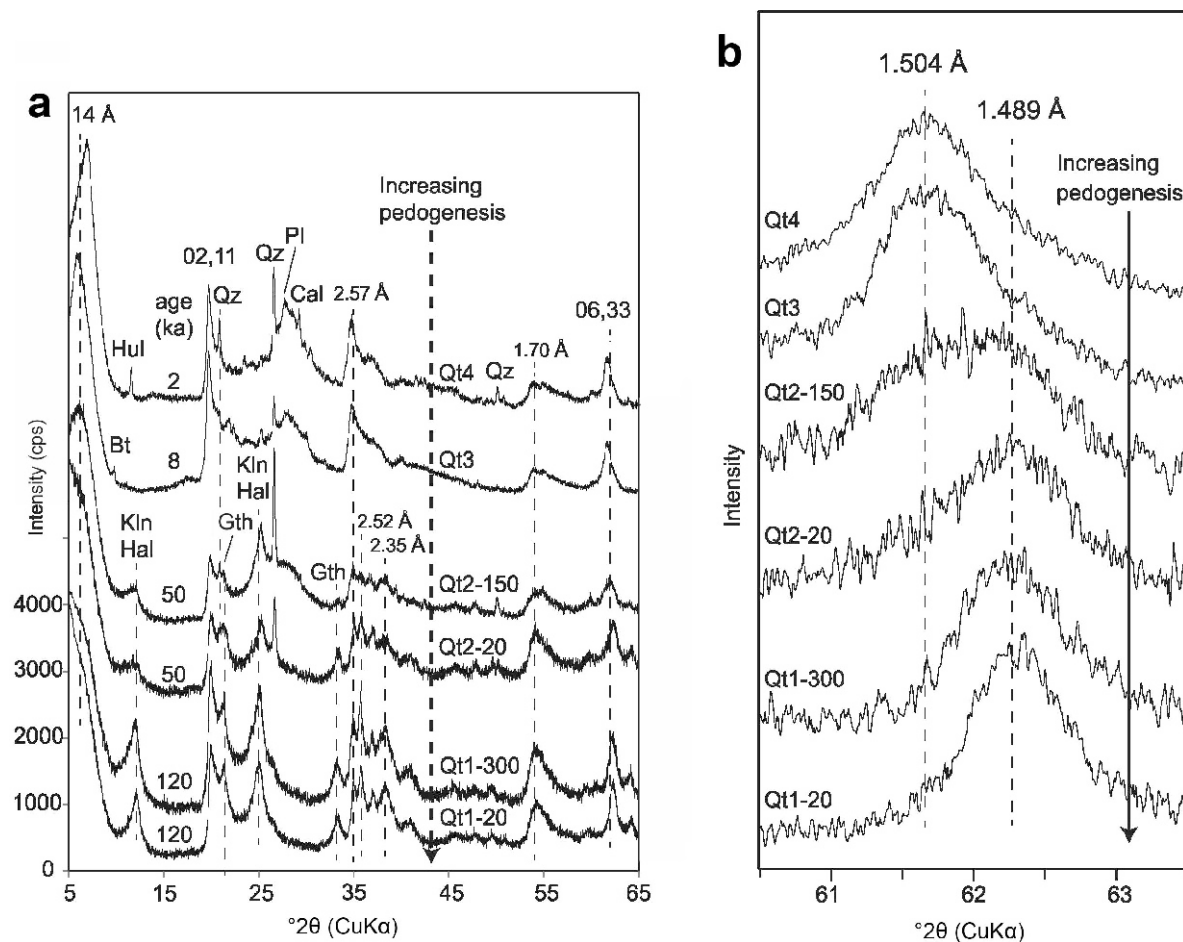

Figure 3. (a) XRD patterns of random mounts of the <2 μm fraction from the youngest and least-evolved soil (top, Qt4) to the oldest and most evolved soil (bottom, Qt1-20). Positions for selected peaks associated with smectite, K-S, halloysite, or kaolinite are shown in Å. Bt = biotite, Qz = quartz, Cal = calcite, Hul = heulandite, Gth = goethite, Kln = kaolinite, and Hal = halloysite. (b) 06,33 region of soil clays arranged from youngest and least-evolved (top) to oldest and most evolved (bottom).
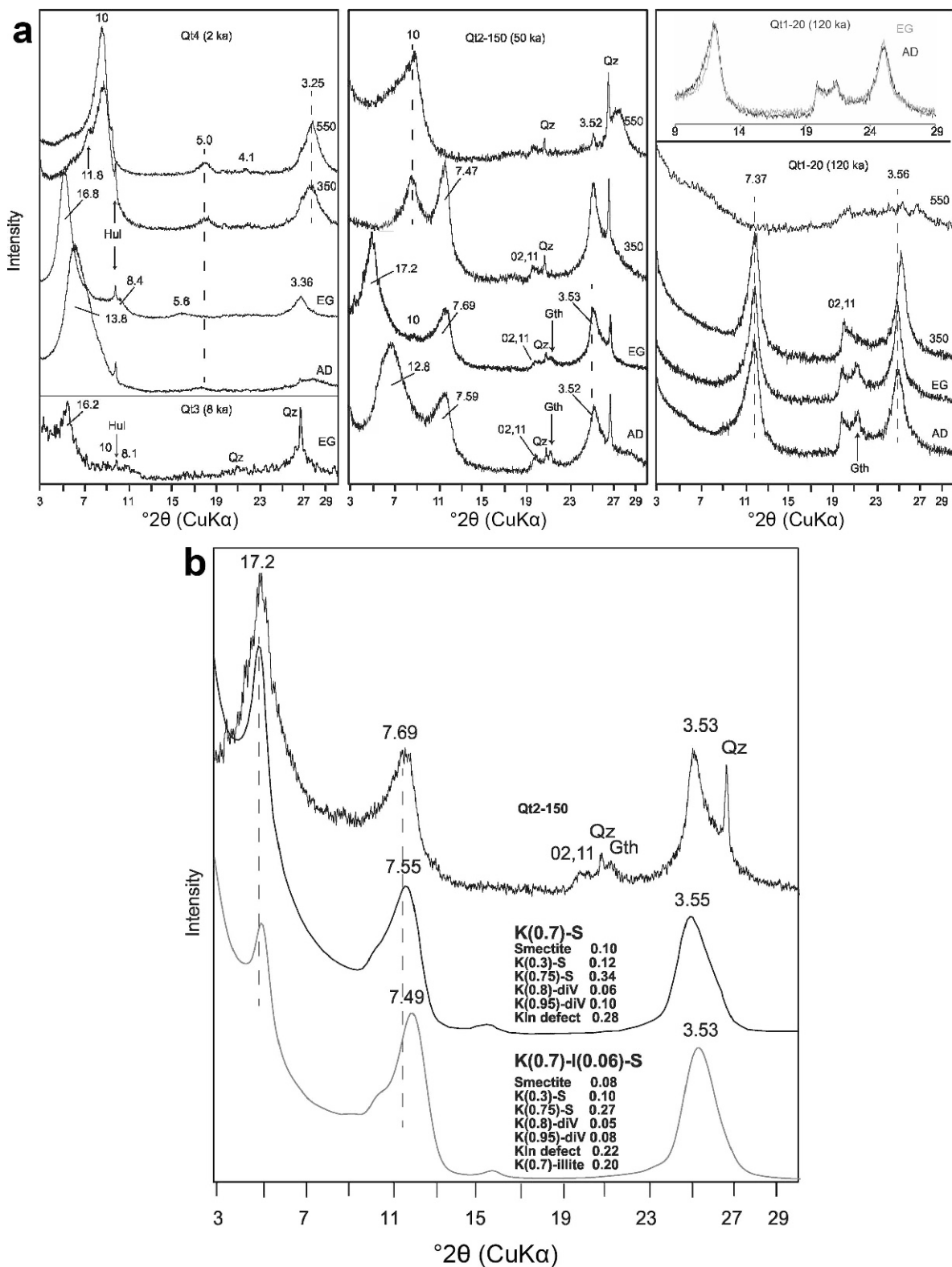
symmetrical 001 peak (EG-saturated specimens) at 16.8 to 16.9 Å with higher order 00*l* peaks at 8.4, 5.6, and 3.36 Å. Qt3 smectite produces a 001 peak at 16.1−16.4 Å that is weaker than the Qt4 001, and which also has a 002 peak at 8.1−8.2 Å. For both Qt4 and Qt3, heating to 350ºC causes collapse of the 001 peak to 10 Å with a secondary peak at ~12 Å and a broad, low-intensity band centered at 14 Å which indicate incomplete collapse of some layers, probably caused by the presence of Al-hydroxy interlayers (Barnhisel and Bertsch, 1989). Further heating to 550ºC caused nearly complete collapse of smectite layers to 10 Å; the eventual collapse is consistent with dehydroxylation of Al-hydroxy interlayer complexes at 550ºC (Barnhisel and Bertsch, 1989). The Al-hydroxy interlayered 2:1 layers observed here will be referred to as hydroxy-interlayer smectite (HIS) given their expandability and origin as pedogenic smectite, but note that they may be genetically related to hydroxy-interlayer vermiculite (HIV), dioctahedral vermiculite, and dioctahedral chlorite observed in soils with high Al activity (Karathanasis and Hajek, 1984; Barnhisel and Bertsch, 1989; Schulze, 2005; Meunier, 2007). No evidence was found of kaolinite or halloysite in these Holocene terrace soils.

Qt2. The occurrence of dioctahedral 7 Å layers (*i.e.* kaolinite or halloysite) in Qt2 soils (50 ka) is indicated by broad asymmetric peaks at ~7.5 and 3.5 Å (Figures 3, 5). The presence of an expandable component is indicated by peaks of varied intensity between 12 and 17 Å that respond to EG solvation. At 150 cm depth (Qt2-150), 00*l* peaks are noticeably irrational − in the air-dried state, broad peaks occurred at 12.8 Å and 7.59 Å, and EG caused these peaks to shift to 17.2 Å and 7.69 Å. These characteristics are consistent with randomly interstratified K-S which contains ~60−70% kaolinite layers (Cradwick and Wilson, 1972; Hughes *et al.*, 1993). A *NEWMOD* model with 70% kaolinite layers occurring in a range of layer types replicates the XRD pattern of Qt2-150 reasonably well (Figure 4b). The asymmetry of peaks in the experimental XRD data is comparable to peak shapes in the model, but the low-angle backgrounds differ, and peak positions of the 7.69 and 3.53 Å (experimental) differ slightly from the model-generated 7.55 and 3.55 Å peaks. The modeled pattern consists of (in order from smectite-rich to
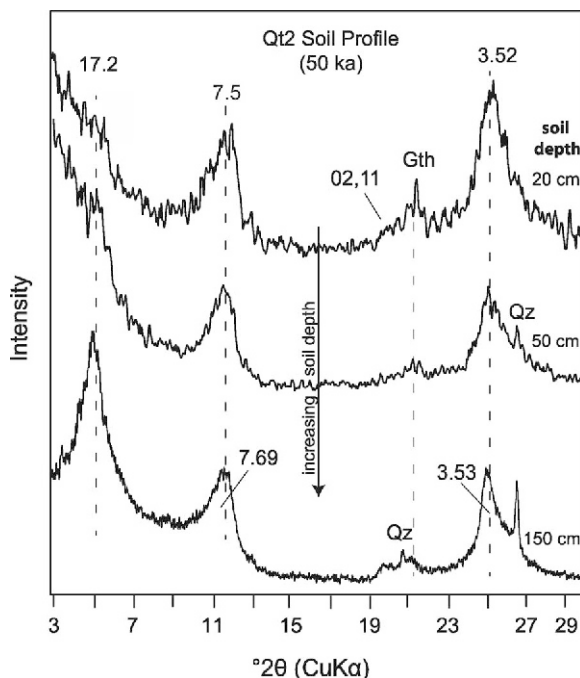

Figure 5. XRD patterns of oriented, EG-solvated <2 µm fractions of soil from 20 cm, 50 cm, and 150 cm depth of the 50 ka Qt2 terrace. Note that a significant portion of the 2:1 to 1:1 transition takes place upward within this single profile of intermediate age.

kaolinite-rich end-members): 10% discrete smectite (0.6 Fe per 2 octahedral sites); 12% R0 K-S with 30% kaolinite layers; 34% R0 K-S with 75% kaolinite layers and dioctahedral Ca-exchanged smectite; 6% R0 kaolinite-dioctahedral vermiculite with 80% kaolinite layers; 10% R0 kaolinite-dioctahedral vermiculite with 95% kaolinite layers; and 28% disordered kaolinite (with mean defect-free distance of 10 and σ* of 5). The dioctahedral vermiculite was used to replicate XRD evidence of Al-hydroxy interlayers. This model is not a unique solution but probably does reflect the general character of the complex interstratifications and physical mixture of layer types in this sample dominated by K-S. Attempts were made to explore the potential effect of interstratified illite layers within the K-S (Figure 4b), but when R0 K-I is included as a component the match with Qt2-150 clay worsens, notably in the weakening of the 001 peak at (17.2 Å) and shift of the 002 peak to 7.49 Å.

Figure 4 (*facing page*). (a) XRD patterns of oriented mounts, from youngest (left) to oldest (right). From bottom to top for each panel: air-dried, EG-solvated, heated to 350ºC, and heated to 550ºC. Qt3 smectite (lower left) is shown in the EG state only. Peak positions are given in Å. Note progression from smectite (left, youngest) to halloysite and kaolinite (right, oldest). Note also the 02,11 peak, the presence of which is due to halloysite. The upper-right panel shows the subtle change that occurs with EG solvation of clay dominated by halloysite and flaky Fe-kaolinite with up to 10% smectite layers. Refer to the caption for Figure 3a for mineral abbreviations. (b) Experimental pattern of Qt2-150 (top) with modeled patterns (EG-solvated state) created using *NEWMOD* (Reynolds, 2012). The model indicated as 'K(0.70)-S' contains 70% kaolinite layers in R0 K-S with Al-hydroxy interlayers but no illite layers. The lower-most pattern (K-I-S) is an example of interstratified and physically mixed clay that contains kaolinite, Ca-smectite, Al-hydroxy-interlayer clay (di-vermiculite), and 6% illite layers. Shown for each model are mineral components included in the model. See text for details.

This is not to say that no illite-like layers are present in the K-S assemblage, but no strong XRD evidence in support of coherent packets of interstratified kaolinite and illite was found.

The presence of a broad 060 peak, rather than distinct 060 peaks of end-member smectite and kaolinite, is more consistent with interstratified K-S than with a physical mixture solely of end-members (Dudek *et al.*, 2006); this is especially evident in the broad 060 peak of Qt2-150 (Figure 3b).

Shallower Qt2 soil (Qt2-20) reveals a weaker and broader peak (EG) centered at ~17 Å (Figure 5), indicating persistence of smectite layers of decreasing abundance (in K-S), and the position of the 001/002 peak at 7.59 Å is consistent with an average of ~85−90% K layers in R0 K-S. The composite character of the 001/002 peak, with sub-peaks at 8.1 Å and 7.3 Å, indicates the coexistence of K-S as well as discrete kaolinite or halloysite. The ~17 Å position of the K-S 001 peak is consistent with the occurrence of Al-hydroxy interlayers − this peak position cannot be modeled with *NEWMOD* unless Al-hydroxy interlayers are present; if modeled with fully expandable 17 Å smectite layers and no vermiculite-like layers, this peak occurs at ~20 Å. The low expand-ability of the Al-hydroxy interlayers shifts this peak to the lower *d* spacing observed. In the 06,33 region of Qt2-20, the greater intensity of the 1.490 Å peak (relative to the 1.504 Å peak) is consistent with increasing kaolinite or halloysite relative to smectite (Qt2-20 is closer to the soil surface than Qt2-150 and thus is more evolved). The 020 peak in Qt2-20 occurs at 4.47 Å and the 060 peak is centered at 1.491 Å (Figure 3b), indicating a *b*-axis dimension of 8.95 Å.

Goethite is present in these 50 ka soils as indicated by peaks at 4.18 and 2.69 Å which disappear after heating to 350ºC. Goethite-like sub-micron-scale clusters of Fe-(oxyhydr)oxide were observed in TEM.

Qt1. The abundance of kaolinite and/or halloysite in the Qt1 samples is indicated by strong and relatively sharp peaks at 7.35−7.41 Å and 3.55−3.58 Å. These peaks are asymmetrical, slightly irrational, and shift slightly with EG solvation and with heating to 350ºC (Figure 4). When these data are modeled with *NEWMOD* they indicate the presence of ~95% K layers and 5% S layers, assuming all crystals are K-S; these results, however, do not distinguish readily whether or not all of the clay is K-S, or whether some is K-S and some consists of discrete 7 Å crystals of kaolinite or halloysite. The TEM results indicate the presence of all three. The occurrence of halloysite is suggested by a slight increase in intensity of the 002 relative to the 001 when treated with EG (MacEwan, 1948; Hillier and Ryan, 2002), and also by the fact that oriented preparations of these samples (or at least attempts to do so) exhibit strong non-00*l* peaks (*e.g.* 02,11 band), suggesting rolled halloysite layers (Figure 4a). The 060 peak occurs at 1.489 Å, indicating a

b-axis dimension of 8.934 Å. The presence of goethite is indicated by relatively strong peaks at 4.18 and 2.69 Å which disappear after heating to 350ºC.

The XRD patterns of a Qt2 soil profile (Figure 5) illustrate the transition from a K-S-dominated assem-blage (at 150 cm depth) to a kaolinite+halloysite-dominated assemblage in the shallower and more evolved Qt2-50 and Qt2-20 soil horizons. An important result of Qt2 profile mineralogy is that it shows much of the chronosequence mineral evolution in a single soil profile that has virtually no variability in parent material (Table 2), from a K-S mineralogy in the deeper part (150 cm) to kaolinite+halloysite-dominated in the upper B-horizon (20 cm).

Single-crystal composition and form (TEM-AEM)

Qt4 and Qt3 (smectite-dominated). Mineral grains in the <2 μm fraction of ≤8 ka soils (B or AB horizons, 2 ka and 8 ka) are dominated by smectites that occur as individual 0.5−2 μm (diameter) flaky crystals, often with wavy or curled edges (Figure 6). No other pedogenic minerals were discovered in Qt4 (including no obvious sign of amorphous solids such as allophane); smectite also dominates the fine-grained solids in Qt3, which did contain one crystal of K-S (Table 3; see below). Weathered grains of plagioclase, clinopyroxene, and accessory apatite and olivine, were observed in Qt4, constituting ~5% of mineral grains observed in Qt4 TEM images, and a Mg-Si-rich weathered grain (presumably of clinopyroxene) was observed in Qt3. Otherwise, the clay fractions of Qt4 and Qt3 are very dominated by flaky crystals of smectite with curled edges. The TEM-AEM compositional analysis detected no interstratified kaolinite layers in the smectites from Qt4; in Qt3, the crystal of K-S was identified by less Si and more Al content than end-member smectite (Tables 3, 4).

Compositional analysis by means of TEM-AEM indicated a relatively small amount of compositional variability in the smectites, much of which was probably due to localized differences in parent-mineral composition (Gaudin *et al.*, 2004; Ryan and Huertas, 2009); notably, interlayers of Qt4 contain $Ca^{2+} > K^+$ whereas interlayers of Qt3 contain $K^+ > Ca^{2+}$ (Table 3). Negative charge on 2:1 layers of −0.4 to −0.5 mol_c per formula unit (p.f.u., based on $O_{10}[OH]_2$) is derived from Al for Si substitution in the tetrahedral sheet (0.1 to 0.2 mol_c p.f.u.) and by Mg for Al in the octahedral sheet. Octahedral occupancy (Al+Fe+Mg) is 2.1−2.2 a.p.f.u., and the overall negative charge derived from the octahedral sheet is 0.2 to 0.3 mol_c p.f.u. Assuming all Fe is ferric, the average smectite crystal in Qt4 derives a negative charge of 0.12 mol_c from the tetrahedral sheet and 0.33 mol_c from the octahedral sheet; in Qt3, average smectite derives 0.18 mol_c from the tetrahedral sheet and 0.21 mol_c from the octahedral sheet. Interlayers contain Ca as well as fixed K and Al; the occurrence of interlayer Al is indicated by XRD, and Al is apportioned into the interlayer of smectite and K-S so that
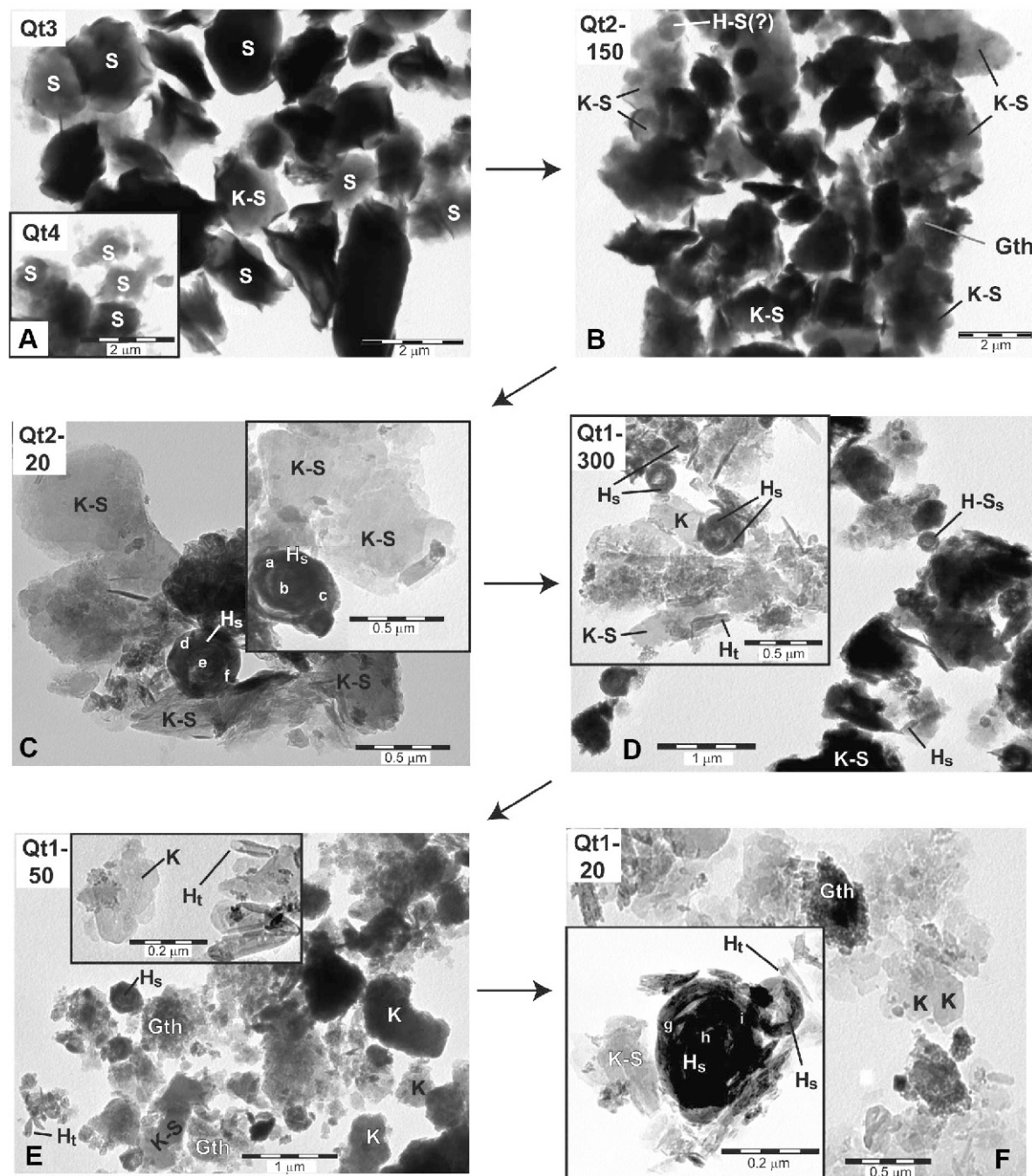
Figure 6. TEM images which document changes in soil mineralogy from Holocene age (≤8 ka) smectite-dominated soils (Qt3) through intermediate-age (50 ka) soils dominated by halloysite and K-S (Qt2) to oldest (120 ka) soils that show signs of incipient formation of hexagonal kaolinite (Qt1). Gth = goethite and Qz = quartz. Mineral abbreviations for the clays are as follows: Sme = smectite, K-S = interstratified kaolinite-smectite, Hs = spheroidal halloysite, Ht = tubular halloysite, H-Ss = spheroidal interstratified halloysite-smectite, and Kln = kaolinite. Lower-case letters (*e.g.* a-b-c, d-e-f, g-h-i) indicate halloysites for which compositions were measured by AEM along cross-crystal transects (see Figure 8).

the sum of charges of Ca^{2+}, K^+, and Al^{3+} is +0.4 (to balance the ~−0.4 charge on the 2:1 layer of Qt4 smectites). This does not provide a perfectly precise speciation of Al and some of the Al apportioned into the interlayer could occur in the octahedral sheet, but at the same time, the XRD data given here and the XRD and DTA data of Ryan and Huertas (2009) provide strong evidence for interlayer Al-hydroxy complexes, *e.g.*

Table 3. TEM-AEM analyses of single crystals (mean, standard deviation) of pedogenic minerals arranged in order of increasing evolution, from smectite-dominated Holocene soils to Pleistocene soils rich in halloysite, K-S, and kaolinite. 'Assemblage' indicates mean composition of all clays measured, regardless of type. Crystal morphologies are indicated: 'flks' = flakes, 'sphr' = spheroids, '~hex' = thin crystals with hexagonal edges (see Figure 6). PM = parent material.

Qt4, Qt3 smectites (one K-S crystal in Qt3)

	Qt-4 flakes Mean	SD	Qt-3 flakes Mean	SD	Qt-3 K-S flake Mean	SD	Assemblage Mean	SD
SiO_2	63.1	1.3	62.8	2.1	58.5	–	62.9	1.8
Al_2O_3	16.3	2.0	19.3	1.7	22.9	–	18.0	2.3
Fe_2O_3	13.3	1.6	10.2	1.4	8.94	–	11.6	2.2
MgO	3.58	1.0	4.98	0.8	4.35	–	4.36	1.1
CaO	2.35	0.8	0.55	0.2	0.56	–	1.40	1.1
K_2O	1.41	0.6	2.27	1.3	4.67	–	1.89	1.1
	N = 8		N = 9		N = 1		N = 18	

Qt2-50 cm

	K-S flakes Mean	SD	Smectite flakes Mean	SD	Assemblage Mean	SD
SiO_2	54.6	2.5	65.0	1.9	58.9	5.8
Al_2O_3	31.7	6.4	23.5	1.6	28.3	6.4
Fe_2O_3	11.4	5.8	6.92	2.1	9.53	5.0
MgO	1.80	1.3	3.45	0.7	2.49	1.3
CaO	0.34	0.2	0.45	0.4	0.38	0.3
K_2O	<0.2	–	0.59	0.7	0.35	0.5
	N = 7		N = 5		N = 12	

Qt1-300 cm

	Halloysite sphr > tube Mean	SD	Kaol, K-S flakes Mean	SD	Kaolinite hex Mean	SD	Assemblage Mean	SD
SiO_2	51.5	1.9	52.3	3.82	49.6	2.9	51.2	2.1
Al_2O_3	41.7	2.3	37.5	2.23	38.5	3.6	40.5	3.1
Fe_2O_3	5.52	1.1	8.39	3.46	10.2	5.0	7.00	3.0
MgO	1.21	0.3	1.45	0.81	1.71	0.5	1.35	0.5
CaO	<0.2	–	0.10	0.27	<0.2	–	<0.2	–
K_2O	<0.2	–	0.34	0.98	<0.2	–	<0.2	–
	N = 12		N = 8		N = 5		N = 21	

Qt1-20 cm

	Kaolinite ~hex Mean	SD	Halloysite tubes = sphr Mean	SD	K-S flakes Mean	SD	Assemblage Mean	SD
SiO_2	53.6	0.2	52.3	1.6	56.5	2.7	54.1	2.4
Al_2O_3	42.4	1.6	41.4	3.4	38.9	2.0	41.3	2.7
Fe_2O_3	2.79	2.0	4.95	1.9	3.52	1.4	3.42	2.2
MgO	1.25	1.0	1.30	0.2	1.11	0.3	1.18	0.7
CaO	<0.2	–	<0.2	–	<0.2	–	<0.2	–
K_2O	<0.2	–	<0.2	–	<0.2	–	<0.2	–
	N = 5		N = 5		N = 3		N = 13	

Qt2-150 cm

	K-S flakes ~hex + flks Mean	SD	Smectite flakes Mean	SD	Assemblage Mean	SD
SiO_2	54.3	3.3	61.1	NA	54.9	3.8
Al_2O_3	30.4	4.4	21.0	NA	29.5	5.0
Fe_2O_3	13.0	4.3	12.3	NA	13.0	4.1
MgO	1.93	1.0	2.29	NA	1.97	0.9
CaO	0.22	0.3	0.28	NA	0.23	0.3
K_2O	<0.2	–	3.04	NA	<0.2	–
	N = 10		N = 1		N = 11	

Qt2-20 cm

	Kaolinite ~hex + flks Mean	SD	Halloysite tubes > sphr Mean	SD	K-S flakes Mean	SD	Assemblage Mean	SD
SiO_2	51.7	1.1	51.8	2.5	55.4	2.9	53.1	2.9
Al_2O_3	38.5	2.0	39.2	3.0	33.5	1.7	36.9	3.5
Fe_2O_3	7.92	2.1	7.84	4.4	8.68	2.8	8.17	3.2
MgO	1.93	0.6	1.20	0.4	2.46	0.9	1.86	0.9
CaO	<0.2	–	<0.2	–	<0.2	–	<0.2	–
K_2O	<0.2	–	<0.2	–	<0.2	–	<0.2	–
	N = 4		N = 6		N = 6		N = 16	

Qt1-50 cm

	Kaolinite ~hex Mean	SD	PM	Halloysite tubes = sphr Mean	SD	K-S flakes Mean	SD	Assemblage Mean	SD
SiO_2	51.8	0.7	51.28	52.9	1.5	54.4	0.3	52.3	0.1
Al_2O_3	41.2	1.6	42.96	41.9	2.8	32.4	1.3	40.4	4.3
Fe_2O_3	5.92	2.6	4.317	4.31	2.5	12.0	1.2	6.36	3.5
MgO	1.00	0.7		0.54	0.6	1.17	0.2	0.89	0.6
CaO	<0.2	–		<0.2	–	0.36	0.5	<0.2	–
K_2O	<0.2	–		<0.2	–	<0.2	–	<0.2	–
	N = 7			N = 4		N = 2		N = 13	

Table 4. TEM single-crystal analyses of pedogenic clays in the Nicoya chronosequence in order of increasing pedogenesis (from top to bottom). K-S formulae are normalized to a smectite unit cell for K-S crystals that are smectite rich (indicated by *), and to a kaolinite unit cell for K-S crystals that are kaolinite rich (indicated by **). Also, some Al is apportioned into interlayers based on XRD and DTA evidence of hydroxy-Al in interlayers and assuming a negative layer charge of ~0.4 mol per $O_{10}(OH)_2$ formula. Clays are Ca-saturated. The numbers of spot analyses per mineral type are given in parentheses.

ID	Depth (cm)	Age (ka)	Mineral type	Mean	High-Fe-Mg end-member	Low-Fe-Mg end-member
Qt4	15	2	Smectite ($N = 8$)	$(Al_{0.01}K_{0.11}Ca_{0.16})(Al_{1.05}Fe_{0.62}Mg_{0.33})$ $(Si_{3.88}Al_{0.12})O_{10}(OH)_2$	$(K_{0.2}Ca_{0.10})(Al_{0.91}Fe_{0.64}Mg_{0.48})$ $(Si_{3.96}Al_{0.04})O_{10}(OH)_2$	$(K_{0.08}Ca_{0.19})(Al_{1.18}Fe_{0.48}Mg_{0.33})$ $(Si_{3.86}Al_{0.14})O_{10}(OH)_2$
Qt3	15	10	Smectite ($N = 9$)	$(Al_{0.05}K_{0.18}Ca_{0.04})(Al_{1.16}Fe_{0.47}Mg_{0.45})$ $(Si_{3.82}Al_{0.18})O_{10}(OH)_2$	$(Al_{0.03}K_{0.20}$ $Ca_{0.04})(Al_{0.93}$ $Fe_{0.62}$ $Mg_{0.45})(Si_{3.78}$ $Al_{0.22})O_{10}(OH)_2$	$(Al_{0.06}K_{0.13}Ca_{0.04})(Al_{1.21}Fe_{0.39}Mg_{0.47})$ $(Si_{3.86}$ $Al_{0.14})O_{10}(OH)_2$
			S-rich K-S ($N = 1$)	* $(K_{0.37}Ca_{0.04})(Al_{1.29}Fe_{0.42}Mg_{0.40})$ $(Si_{3.62}Al_{0.38})O_{10}(OH)_2$	– (only 1 specimen identified in TEM)	– (only 1 specimen identified in TEM)
Qt2	150	40	K-S ($N = 10$)	* $(Al_{0.11}K_{0.03}Ca_{0.01})(Al_{1.37}Fe_{0.60}Mg_{0.18})$ $(Si_{3.35}Al_{0.65})O_{10}(OH)_2$	* $(Al_{0.12}K_{0.03}Ca_{0.01})(Al_{1.29-}$ $Fe_{0.84}Mg_{0.29})(Si_{3.26}Al_{0.74})O_{10}(OH)_2$	* $(Al_{0.12}K_{0.04})(Al_{1.88}Fe_{0.23})$ $(Si_{3.32}Al_{0.68})O_{10}(OH)_2$
			Smectite ($N = 1$)	$(Al_{0.09}K_{0.03}Ca_{0.06})(Al_{1.22}Fe_{0.57}Mg_{0.21})$ $(Si_{3.78}Al_{0.22})O_{10}(OH)_2$	– (only 1 specimen identified in TEM)	– (only 1 specimen identified in TEM)
Qt2	20	40	Hal sph ($N = 6$)	$(Al_{1.74}Fe_{0.22}Mg_{0.07})$ $(Si_{1.98}Al_{0.02})O_5(OH)_4$	$(Al_{1.59}Fe_{0.41}Mg_{0.06})(Si_{1.86}Al_{0.14})$ $O_5(OH)_4$	$(Al_{1.86}Fe_{0.11}Mg_{0.03})(Si_{2.00})O_5(OH)_4$
			K-rich K-S ($N = 6$)	* $Al_{0.13}$ $(Al_{1.48}Fe_{0.39}Mg_{0.22})$ $(Si_{3.28}Al_{0.72})O_{10}(OH)_2$	* $Al_{0.13}(Al_{1.25}Fe_{0.52}Mg_{0.25})(Si_{3.22}Al_{0.78})$ $O_{10}(OH)_2$	* $Al_{0.13}(Al_{1.79}Fe_{0.18}Mg_{0.09})(Si_{3.50}Al_{0.50})$ $O_{10}(OH)_2$
			Kaol flaky ($N = 4$)	$(Al_{1.71}Fe_{0.23}Mg_{0.11})(Si_{1.98}Al_{0.02})$ $O_5(OH)_4$	$(Al_{1.62}Fe_{0.29}Mg_{0.16})(Si_{1.96}Al_{0.04})$ $O_5(OH)_4$	$(Al_{1.80}Fe_{0.15}Mg_{0.08})(Si_{1.98}Al_{0.02})$ $O_5(OH)_4$
Qt1	300	120	Kaol/K-S flaky ($N = 11$)	** $(K_{0.02}Ca_{0.01})(Al_{1.66}Fe_{0.27}Mg_{0.07})$ $(Si_{2.01})O_{10}(OH)_2$	** $(Al_{1.50}Fe_{0.45}Mg_{0.11})(Si_{1.91}Al_{0.09})$ $O_5(OH)_4$	* $Al_{0.13}$ $(Al_{1.77}Fe_{0.20}Mg_{0.13})(Si_{3.44}Al_{0.56})$ $O_{10}(OH)_2$
			Hal sph ($N = 9$)	$(Al_{1.81}Fe_{0.16}Mg_{0.07})(Si_{1.95}Al_{0.05})$ $O_5(OH)_4$	$(Al_{1.80}Fe_{0.18}Mg_{0.09})(Si_{1.89}Al_{0.11})$ $O_5(OH)_4$	$(Al_{1.86}Fe_{0.14}Mg_{0.04})(Si_{1.92}Al_{0.08})$ $O_5(OH)_4$
			K hex or lath ($N = 5$)	$(K_{0.04}Ca_{0.01})(Al_{1.80}Fe_{0.16}Mg_{0.04})$ $(Si_{1.98}Al_{0.02})O_{10}(OH)_2$	** $Ca_{0.02}$ $(Al_{1.75}Fe_{0.17}Mg_{0.08})(Si_{2.01})$ $O_5(OH)_4$	** $(Al_{1.83}Fe_{0.14}Mg_{0.02})(Si_{2.01})$ $O_5(OH)_4$
			Hal tube ($N = 3$)	$Ca_{0.02}$ $(Al_{1.81}Fe_{0.15}Mg_{0.05})(Si_{1.98}Al_{0.02})$ $O_5(OH)_4$	$(Al_{1.76}Fe_{0.21}Mg_{0.06})(Si_{1.98}Al_{0.02})$ $O_5(OH)_4$	$(Al_{1.89}Fe_{0.09}Mg_{0.07})(Si_{1.92}Al_{0.08})$ $O_5(OH)_4$
Qt1	20, 50	120	Kaol/K-S flaky ($N = 10$)	** $(Al_{1.73}Fe_{0.21}Mg_{0.07})(Si_{2.01})O_5(OH)_4$	$(Al_{1.65}Fe_{0.30}Mg_{0.09})(Si_{1.95}Al_{0.05})$ $O_5(OH)_4$	* $Al_{0.13}$ $(Al_{1.90}Fe_{0.09}Mg_{0.11})(Si_{3.39}Al_{0.61})$ $O_{10}(OH)_2$
			K hex or lath ($N = 6$)	** $(Al_{1.84}Fe_{0.08}Mg_{0.06})(Si_{2.02})O_5(OH)_4$	** $(Al_{1.86}Fe_{0.13})(Si_{2.01})$ $O_5(OH)_4$	$(Al_{1.95}Fe_{0.02}Mg_{0.04})(Si_{2.00})$ $O_5(OH)_4$
			Hal sph ($N = 5$)	$(Al_{1.79}Fe_{0.17}Mg_{0.06})(Si_{1.98}Al_{0.02})$ $O_5(OH)_4$	$(Al_{1.77}Fe_{0.18}Mg_{0.09})(Si_{1.96}Al_{0.04})$ $O_5(OH)_4$	$(Al_{1.82}Fe_{0.14}Mg_{0.06})(Si_{2.00})$ $O_5(OH)_4$
			Hal tube ($N = 5$)	$(Al_{1.90}Fe_{0.08}Mg_{0.04})(Si_{1.96}Al_{0.04})$ $O_5(OH)_4$	$(Al_{1.82}Fe_{0.13}Mg_{0.07})(Si_{2.00})$ $O_5(OH)_4$	$(Al_{1.98}Fe_{0.04})(Si_{1.92}Al_{0.08})$ $O_5(OH)_4$

hydrated $Al(OH)_2^+$, and quantifying interlayer Al in HIS as well as possible is important, given these constraints (Meunier, 2007).

Qt2-150, kaolinite-smectite-dominated. The dominant clay at 150 cm depth (C-horizon, 50 ka) in intermediate-age Qt2 is interstratified K-S with 70 ± 10% K layers. Only one crystal of discrete smectite was identified (Table 4) and other than one fuzzy spherical crystal whose intermediate composition implies halloysite-smectite (upper left of Figure 6B), all crystals are K-S. The approximate ratio of kaolinite layers to smectite layers in K-S crystals was estimated, given compositions of end-member smectite and kaolinite (Table 4). Based on Al_2O_3, and given that end-member smectite contains 18.0% Al_2O_3 and flaky Fe-kaolinite from Qt2-20 contains 38.5% Al_2O_3, the 30.4% Al_2O_3 in K-S (from Qt2-150) indicates ~60% kaolinite layers. In a similar way, based on SiO_2, Qt2-150 K-S contains 75% K layers; based on MgO, the K-S contains 80% K layers. These estimates are reasonably consistent with XRD and a *NEWMOD* model indicating 70% K layers.

Qt2-20, curled flaky K-S > spheroidal halloysite > curled flaky kaolinite. The dominant clay in Qt2-20 (upper B-horizon, 50 ka) is individual 0.5−2 μm (diameter) flaky crystals of K-S with 80−90% kaolinite layers. Spheroidal halloysites 0.2−0.5 μm in diameter are approximately one-half the abundance of curled, flaky K-S. Relative to coexisting K-S, the halloysites are enriched in Al and depleted in Si, Fe, and Mg (Tables 3, 4). Kaolinite constitutes ~10% of the clay fraction of Qt2-20 and occurs predominantly as flaky crystals with similar form to smectite and K-S, and less commonly as <0.2 μm hexagonal crystals; flaky kaolinite is texturally similar to K-S, is compositionally more similar to halloysite (note: "halloysite" is defined here as spheroidal or tubular crystals and "kaolinite" as flaky or platy crystals; Hart *et al.*, 2002).

Qt1-300, curled, flaky K-S > spheroidal halloysite > tubular halloysite = platy, hexagonal kaolinite. Spheroidal halloysite and flaky K-S and kaolinite with curled edges account for two-thirds of the crystal types observed in the clay fraction of Qt1-300 (deep B or BC horizon, 120 ka). The remaining one-third is sub-equal amounts of very fine-grained tubular halloysite (~0.2 μm long) and platy, hexagonal kaolinite (<0.2 μm long axis). Spheroidal halloysite is enriched in Al and depleted in Fe and Mg relative to spheroidal halloysite in younger Qt2 soil. Tubular halloysite is compositionally similar to spheroidal halloysite; both are enriched in Al and depleted in Fe and Mg relative to coexisting K-S and flaky kaolinite with curled edges (presumably derived from K-S). Compared to K-S and flaky kaolinite (which lack linear crystal edges and 60° intersections), the platy hexagonal kaolinite is morphologically distinct (it is
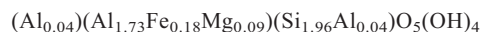
euhedral with hexagonal intersections and no curling at the edges), it is finer-grained, and is translucent in TEM; compositionally, the platy hexagonal kaolinite is very similar to the halloysites in Qt1-300.

Qt1-20 and 50, flaky Fe-kaolinite > halloysite [spheroidal, tubular] > platy hexagonal kaolinite. Qt1-20 and Qt1-50 are combined here and in Table 4 because of their similar content and composition. Halloysite and flaky kaolinite with curled edges constitute ~90% of clay crystals in these, the most-evolved soils of this chronosequence (upper B horizon, ≤50 cm depth, 120 ka). Very fine-grained platy hexagonal kaolinites (<0.2 μm long axis) also occur and constitute ~5−10% of this soil. Numerous crystals with morphologies similar to flaky smectite and K-S with curled edges, but with compositions that are consistent with iron-bearing kaolinite, are referred to here as "Fe-kaolinite" (defined as ≥0.1 mol Fe per $O_5(OH)_4$ formula unit or ≥3% Fe_2O_3; Petit and Decarreau, 1990; Iriarte *et al.*, 2005). Compositionally, one-third of Fe-kaolinites have a slight excess of Si such that when cast as kaolinite they contain >2.00 Si per $O_5(OH)_4$ formula unit; those data, combined with XRD data indicating a small amount of interstratified smectite, are consistent with the persistence of crystals of Fe-kaolinite that still contain up to 10% smectite layers. The Fe-kaolinites (including ones with up to 10% smectite layers) are the least evolved compositionally of clay types in Qt1-20 and Qt1-50, with less Al and more Fe than halloysites or platy hexagonal kaolinites. The most evolved crystal types (*i.e.* enriched in Al, depleted in Fe and Mg) are tubular halloysite and platy hexagonal kaolinite (a minority of which also contain up to 10% interstratified smectite layers). Compositionally, spheroidal halloysite in this soil is intermediate to curled, flaky Fe-kaolinite on one end (less evolved) and tubular halloysite and hexagonal kaolinite on the other (more evolved).

Similar to smectite and K-S, no unique solution exists to the speciation of Al in halloysite. Two ways to cast $O_5(OH)_4$ unit cell formulae for the same spheroidal halloysite from Qt1-20 (Table 4) are:

$$(Al_{1.77}Fe_{0.18}Mg_{0.09})(Si_{1.96}Al_{0.04})O_5(OH)_4$$

or

$$(Al_{0.04})(Al_{1.73}Fe_{0.18}Mg_{0.09})(Si_{1.96}Al_{0.04})O_5(OH)_4$$

The former assumes that all Al is in tetrahedral and octahedral sheets, whereas the latter assumes the presence of Mg_{oct} and Al_{tet} creates a negative layer charge of 0.13 mol, which is satisfied by adsorption of positively charged Al-hydroxy complexes.

Trends in compositions of single crystals vs. bulk-soil chemistry. Analysis of single crystals by TEM-AEM indicates that, over time, the clay-mineral assemblage experiences decreasing Ca, K, Mg, Fe, and Si; of the

major cations, only Al increases in the clay assemblage over time (Figure 7). Given that clays were washed with $CaCl_2$, some Ca^{2+} may not have been present in the clay initially (although given high Ca in parent material, smectite interlayers are probably Ca-rich), but either way it occurs in the interlayer or sorbed to other exposed surfaces. K^+ is presumably bound too well in interlayers to have been removed by Ca^{2+} washing.

While TEM-AEM indicates that Fe decreases over time in clay crystals, ICP-AES data indicate that Fe increases in bulk soil (<2 mm) over time. This descrepancy is attributed to the progressive loss of Fe from clay octahedral sites and its subsequent sequestration in soil by means of incorporation into goethite; by comparison, Ca, K, Mg, and Si are leached from soil, causing their abundances to decrease with increasing age (although some Si is re-apportioned into tetrahedral sheets, so its rate of decrease is lower).

Morphology and composition of halloysites. Compositions of spheroidal halloysites were measured along three transects from crystal center to crystal perimeter (Figure 8). For all three crystals probed this way, Al and Fe are inversely correlated and they suggest a spatial trend where the centers of the spheroidal halloysites are more Al-rich and Fe-poor than at the perimeters. For the transect a-b-c (Figure 8, Qt2-20), the center of the crystal contains 6% Fe_2O_3 while the perimeter contains 14% Fe_2O_3. This trend is less

pronounced in transects d-e-f and g-h-i but is still present.

An image from part of a single crystal of spheroidal halloysite (Figure 9) reveals clearly the presence of only 1:1 (7 Å) layers in the outer half of the crystal, but the inner half of the crystal (within the rectangle in Figure 9b) reveals spacings which suggest the presence of interstratified 1:1 and 2:1 (~12 Å) layers. Increased predominance of 1:1 layers (and decrease of 2:1 layers) progressing outward from cores to rims of halloysite spheroids was also noted by Delvaux *et al.* (1992).

Fourier-transform infrared spectroscopy

The FTIR data are consistent with the progressive transition of smectite to kaolinite or halloysite (Figure 10). The broad band at ~3400 cm^{-1} in Qt4 and to a lesser extent in Qt3 corresponds to OH-stretching vibrations of interlayer water, consistent with the predominance of smectite layers in these young soils. In the FTIR spectrum of Qt3, peaks at 3698 and 3622 cm^{-1} are consistent with XRD and TEM-AEM
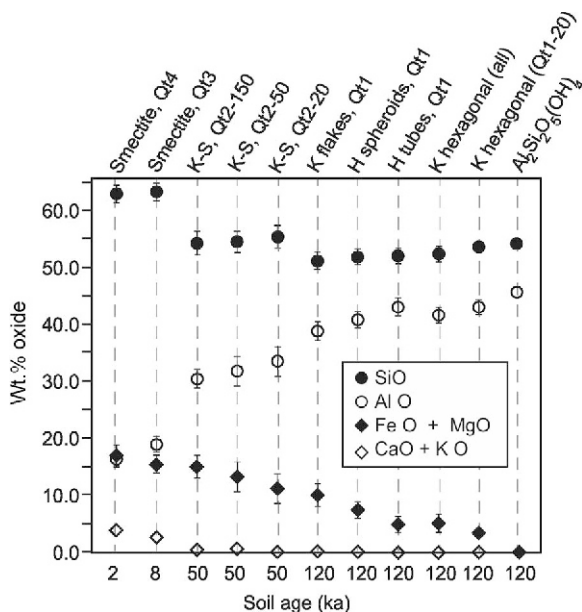

Figure 7. Changes in crystal chemistry from TEM-AEM analysis. Data are arranged from the youngest soil (left) to the oldest (right), with stoichiometric end-member kaolinite on the far right. Note the decreasing Fe, Mg, Ca, and (in a stepwise fashion) Si in the clay crystals over time, and simultaneous increase in Al over time.
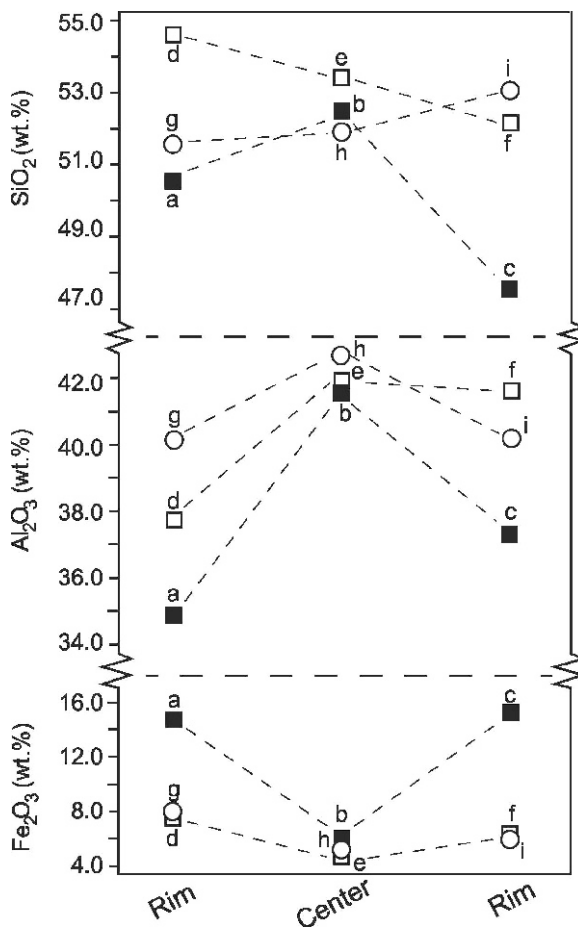

Figure 8. Spot analyses across spheroidal halloysites probed by TEM-AEM. Note that in each case the crystal is more Fe-rich and Al-poor in the rim than in the center.
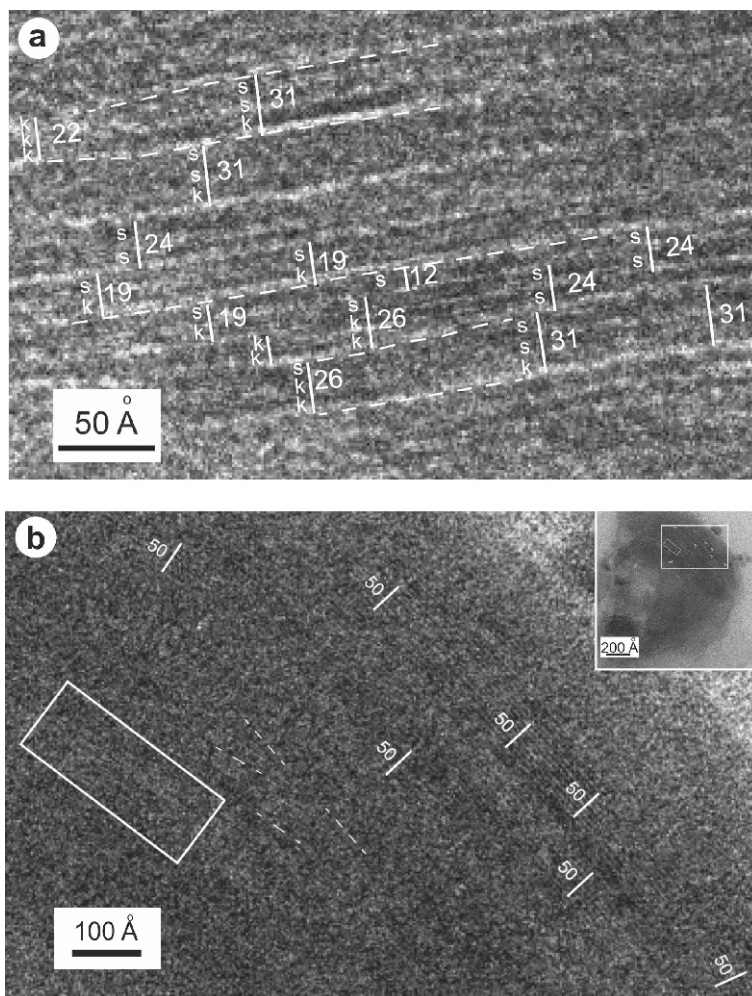
Figure 9. HRTEM images of (a) K-S from Qt2-150 and (b) spheroidal halloysite from Qt1-20.

indications of incipient formation of halloysite or kaolinite layers (Russell and Fraser, 1994). The presence of octahedral Fe, especially in Qt4 smectite, is indicated by the Al-OH-Fe bending band at 870 cm^{-1}, and octahedral Mg, especially in Qt3 smectite, is suggested by the weak Al-OH-Mg band at ~840 cm^{-1} (Dudek *et al.*, 2007). These FTIR-based compositional observations are consistent with TEM-AEM evidence for Fe_{oct} and Mg_{oct} in Qt4 and Qt3 smectite crystals.

Increased intensity of the 3698 and 3622 cm^{-1} peaks in Qt2 clays relative to Qt4 and Qt3 (where these peaks are very weak or absent), and the appearance of a peak at 3653 cm^{-1} in the OH-stretching region, support XRD and TEM evidence of increased abundance of 7 Å dioctahedral layers (halloysite or kaolinite) in these intermediate-age soils. Similarly, peaks at 1103, 1035, 1008, 913, and 694 cm^{-1} in the OH-bending region also indicate increasing kaolinite or halloysite with time. The continued presence of Fe in octahedral sheets is indicated by the Al-OH-Fe bending band at 870 cm^{-1},

and the broad band at ~3400 cm^{-1} is consistent with the presence of smectite layers in interstratified K-S, which is also indicated by XRD and TEM-AEM data.

Progressing to Qt1, increasingly sharper peaks at 3698 and 3622 cm^{-1} (OH-stretching region) and at 1103, 1035, 1008, 913, 798, 751, and 694 cm^{-1} (OH-bending region) reflect increasing kaolinite and halloysite content with soil aging. The presence of the 3653 cm^{-1} peak in the OH-stretching region plus the doublet at 1035 and 1008 cm^{-1} suggest the presence of kaolinite layers (Churchman *et al.*, 1994), although Watanabe *et al.* (1992) showed similar IR spectra for halloysite. Distinction between halloysite and kaolinite is very difficult to achieve using FTIR (Joussein *et al.*, 2005) so in the present study TEM-AEM was found to be more useful than FTIR in this regard. The persistence of the OH-bending peak at 870 cm^{-1} corroborates the presence of octahedral Fe observed in TEM-AEM analyses of kaolinite and halloysite single crystals in Qt2 and Qt1.
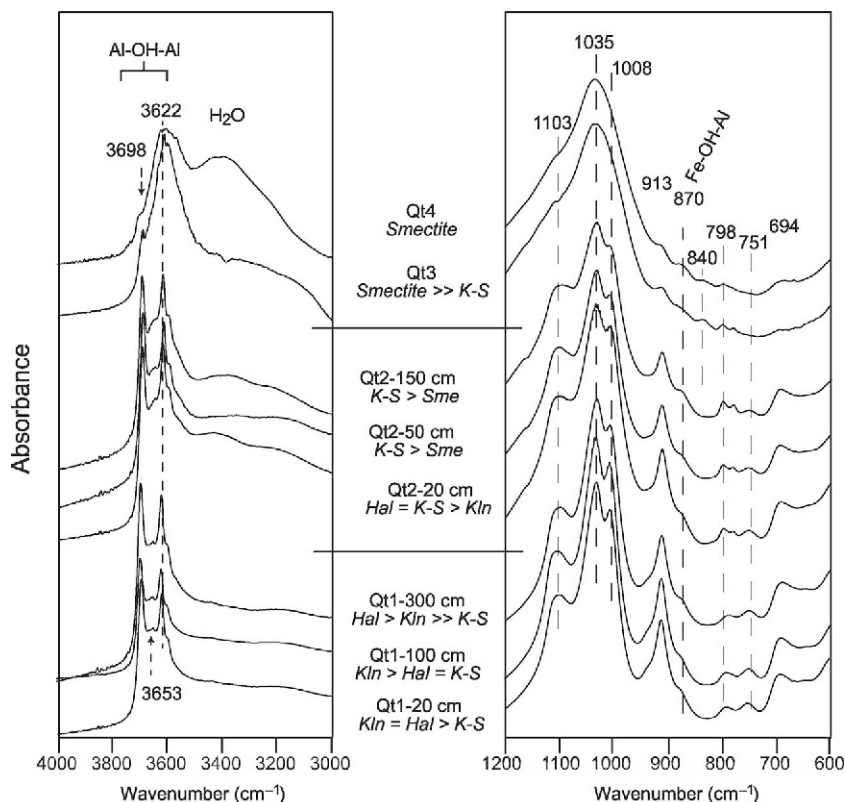
Figure 10. OH-stretching and OH-bending regions of FTIR spectra, from smectite-rich (top) to K-S-dominated (center) to halloysite- and kaolinite-rich (bottom). Peak positions are in cm^{-1}. Sme = smectite, K-S = kaolinite-smectite, Hal = halloysite, Kln = kaolinite.

DISCUSSION

With increasing soil age, early pedogenic smectite (the dominant mineral in ≤ 8 ka soils) has transformed interstratified K-S (with 60−90% kaolinite layers) and spheroidal halloysite, which are the dominant minerals in 50 ka soils. In 120 ka soils, Fe-bearing flaky kaolinite (with <10% smectite interlayers) occurs along with tubular and spheroidal halloysite and incipient hexagonal kaolinite. These changes occur in conjunction with decreasing CEC, Si, and base cations. If the alteration sequence observed in this study is to be useful for understanding and modeling tropical soil, the factors responsible must be quantified as well as possible. As stated in the Introduction, the main factor controlling the variations observed is time, and the evolution of the clay mineral assemblage of this 120 ka chronosequence can be divided into five stages (Figure 11).

Stage 1. Smectite-dominated

The earliest stage of soil formation consists of smectite crystallization in pores and on the surfaces of decomposing beach sediment parent material consisting of plagioclase and clinopyroxene, with lesser amounts of heulandite, mica, volcanic glass, and traces of apatite and olivine. Ca^{2+} from weathered calcite and plagioclase and K^+ from weathered mica are incorporated into

smectite interlayers. With the exception of very small amounts of incipient K-S in Qt3 soils (8 ka), pedogenic smectite is the dominant clay and the only notable pedogenic mineral in Holocene soils. The 8 ka of soil maturation during the Holocene has caused preferential leaching of Ca^{2+}, resulting in 8 ka (Qt3) smectites with greater interlayer K^+ relative to Ca^{2+}.

Stage 2. K-S-dominated

The next stage in pedogenesis is represented by the C-horizon from 50 ka Qt2 (150 cm depth), where the clay assemblage is almost entirely K-S with 60−80% kaolinite layers. Interlayer K^+ and Al-hydroxy complexes appear to be more abundant than interlayer Ca^{2+}.

Stage 3. K-S plus halloysite

Increasing in soil evolution, the 50 ka B-horizon (Qt2-20) consists of K-S with 80−90% kaolinite layers as well as spheroidal halloysites (at approximately one-half the abundance of K-S, based on TEM observations).

Stage 4. Kaolinite, halloysite, K-S

The deep B-horizon (300 cm) sample from 120 ka Qt1 represents the next stage in soil evolution. Fe-kaolinite (with ≤10% smectite layers) is the most abundant clay type as the clay reaction sequence
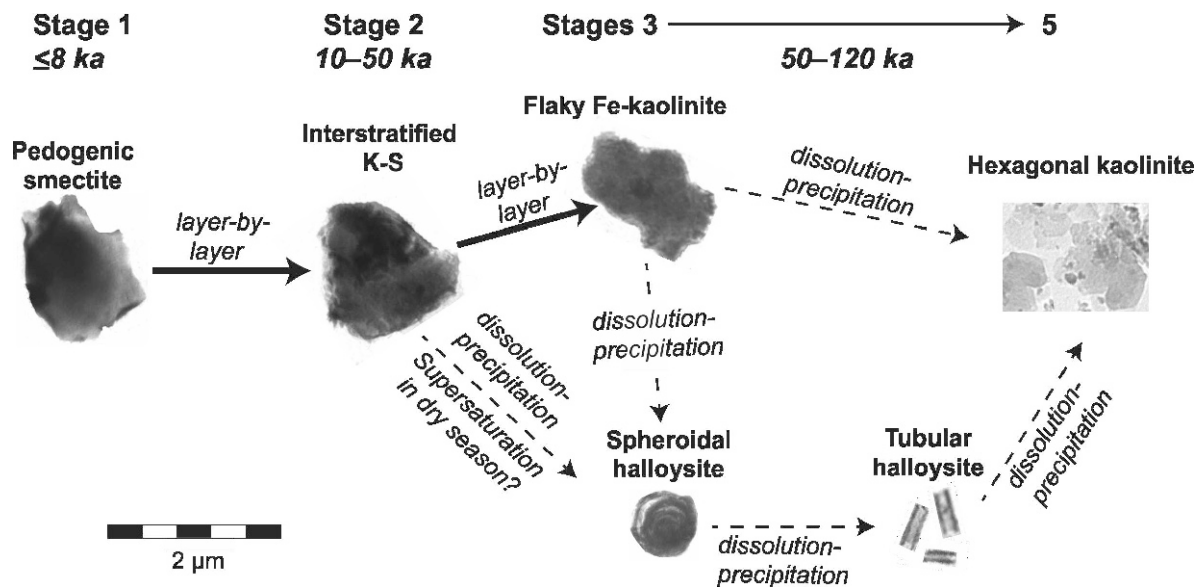
Figure 11. Schematic diagram of the evolution of the clay-mineral assemblage over time.

continues to evolve toward end-member $Al_2Si_2O_5(OH)_4$ kaolinite. Spheroidal halloysite is also abundant, and the first appearances of tubular halloysite and hexagonal kaolinite are observed.

Stage 5. Kaolinite, halloysite

The most abundant mineral in the most evolved soil (Qt1-20 and 50) is flaky Fe-kaolinite which in some crystals could be termed K-S with up to 10% smectite layers. Spheroidal and tubular halloysite occur also, as do sub-micron crystals of low-Fe hexagonal kaolinite.

Considered in terms of thermodynamic data, the progression proceeds as follows: (1) from kinetically favored minerals (initially smectite, then K-S, and later Fe-kaolinite and halloysite) to (2) the thermodynamically favored mineral present in the assemblage, <1 μm diameter, hexagonal crystals of Fe-poor, Al-rich kaolinite.

Given the high molar ratio of Si to Al in pedogenic smectite (~2:1), and the propensity of Si to decrease over time due to leaching in moist tropical soil, smectite rapidly becomes unstable (Tardy and Roquin, 1992); in this system, smectite appears to persist for ~10,000 y, after which increasing Al:Si favors formation of aluminous 1:1 layers (first in K-S, then in halloysite and kaolinite). Regarding kaolinite and halloysite stability, standard free energy of formation (from elements, at 298 K) for kaolinite is -3799 ± 6 kJ/mol, and for halloysite is -3777 ± 6 kJ/mol, values obtained by calorimetric experiments (De Ligny and Navrotsky, 1999). Dean (1979) reported a similar 19 kJ/mol difference in ΔG between halloysite and kaolinite. This being the case, halloysite is a kinetically favored, thermodynamically unstable precursor to kaolinite. Thus, thermodynamic considerations are consistent

with the progression of smectite to interstratified K-S, then to halloysite, and ultimately, to kaolinite. The intermediate MAP of the sequence studied (2800–3200 mm/y) probably contributes to the stabilizing of kaolinite and preventing the system from progressing toward gibbsite, as has been observed in wetter systems (*e.g.* $\geqslant$ 4000 mm/y; Hughes, 1980; Kautz and Ryan, 2003). As noted by Tardy and Roquin (1992), the ratio of Al:Si often stabilizes at a 1:1 molar ratio in moist tropical soil.

If hexagonal end-member $Al_2Si_2O_5(OH)_4$ kaolinite is the thermodynamically stable mineral in moist tropical soils, then the evolving composition of the soil solution appears to be the main factor responsible for kinetically favored crystallization of smectite, K-S, halloysite, and Fe-kaolinite. Evidence for compositional control is indicated by the similarity in composition of soil clays and bulk soil; note parallel and almost overlapping curves for the molar ratios of Al:Si and Al:Mg in bulk soil and in the clay minerals (Figure 12). On a molar basis, the Al:Si ratios are very similar for Holocene bulk soil (<2 mm fraction, $\leqslant$ 8 ka) and single crystals of early-stage smectite (0.26 *vs.* 0.30); likewise, Qt1 soil (<2 mm fraction, 120 ka) has an Al:Si ratio of 0.75 and single crystals of hexagonal kaolinite in Qt1 have Al:Si of 0.91. A similar trend occurs with Al:Mg, where the composition of bulk soil and the clay-mineral assemblage track each other. The only structural element that does not occur in clays in proportion to its abundance in bulk soil is Fe; this is because its abundance in clay minerals decreases progressively (in association with stages of the smectite-to-kaolinite reaction series) while in bulk soil it increases (like Al, the residual amount of Fe increases as other elements are leached out of soil). Rather than being leached when released to solution by
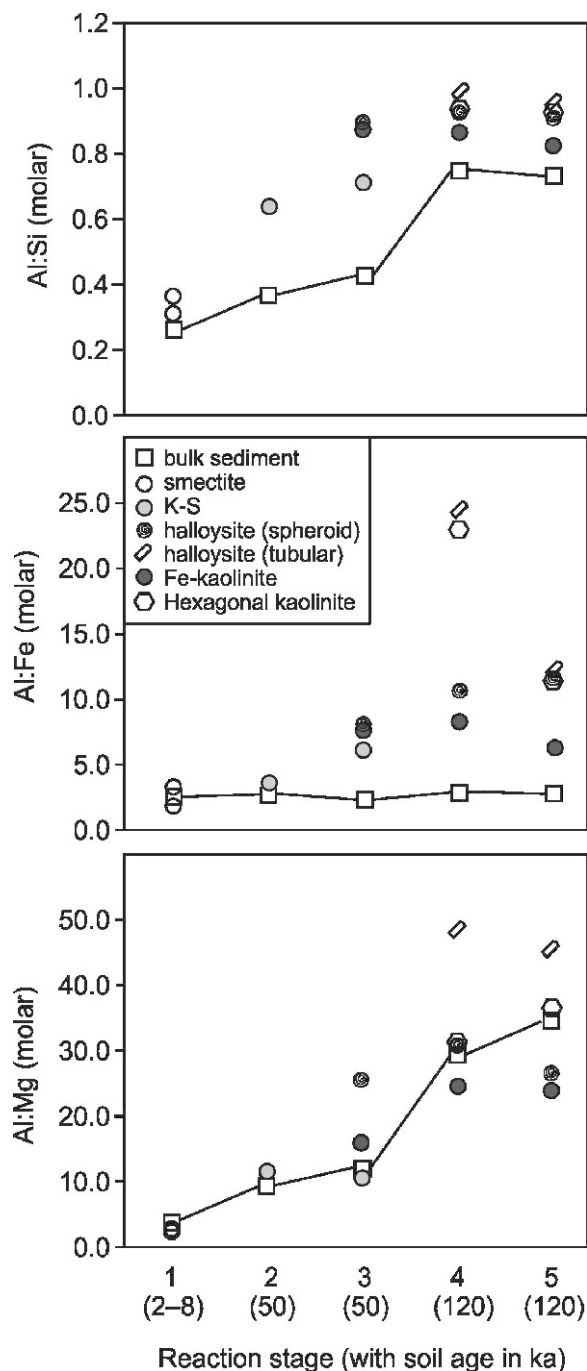
Figure 12. Composition of bulk soil (<2 mm fraction) compared to average compositions of single crystals. Bulk composition and clay-mineral compositions are very similar for all elements other than Fe (an effect of the partitioning of Fe, over time, into goethite).

mineral reaction (as are Mg and Si), Fe is incorporated into goethite. The relatively weak Mg−O bond (362 kJ/mol) and Fe−O bond (409 kJ/mol) relative to the Al−O bond (511 kJ/mol) in octahedral coordination (Newman and Brown, 1987) indicate that Fe and Mg will

be leached preferentially out of octahedral sheets and that Al will be stable in clay octahedral sheets relative to Fe and Mg, consistent with the observed progression.

Two reaction pathways: transformation vs. neoformation

Based on lateral transitions of 2:1 and 1:1 layers observed in HRTEM, the reaction of smectite layers to kaolinite layers (in interstratified K-S) occurs by means of layer-by-layer, localized dissolution-precipitation reactions, *i.e.* by dissolution of a smectite layer, or partial dissolution of a smectite layer, followed by *in situ* formation of a kaolinite layer within the same intact crystal. This transformation reaction is driven by low activity of Si in the soil solution (due to leaching), and evidence for the layer-by-layer reaction mechanism is two-fold: (1) HRTEM lattice fringe images (Figure 9) which indicate lateral transitions of smectite to kaolinite layers within K-S crystals; and (2) smectite crystal habit which is inherited by K-S and persists all the way up to Fe-kaolinite (including K-S with <10% residual smectite layers). This sort of cell-preserved, layer-by-layer transformation mechanism in K-S has also been indicated by HRTEM analyses of Amouric and Olives (1998), Dudek *et al.* (2006), and Ryan and Huertas (2009). The cell-preserved dissolution-precipitation reaction probably occurs within a very local environment (*e.g.* on the scale of 1 to 100 nm), a mechanism which tends to preserve more of the composition of the precursor layer than would wholesale dissolution and precipitation (neoformation); in this study, the crystals of flaky K-S and Fe-kaolinite with curled edges that are present at each reaction stage are closer to the composition of early-stage smectite (*i.e.* have more Fe and Mg) than they are to co-existing halloysite and hexagonal kaolinite. This suggests a different reaction mechanism for the formation of halloysite compared to those of K-S and Fe-kaolinite.

The spheroidal halloysites in Qt2 and Qt1 are derived from precursor smectite or K-S, an assertion supported by the absence of parent material in Qt2 and Qt1 soil (other than detrital quartz grains, no primary minerals were detected by TEM and XRD, *i.e.* little or no parent material remains in Qt2 to form halloysite, therefore halloysite is derived from precursor soil clay). Dissolution of flaky K-S crystals followed by *de novo* crystallization (neoformation) of spheroidal halloysite is consistent with the pronounced morphological change from flaky K-S to spheroidal halloysite, and also with the more evolved composition of spheroidal halloysite relative to Fe-kaolinite − the spheroidal halloysites are more Al-rich and Fe-depleted than Fe-kaolinite, and are farther, compositionally, from K-S than are Fe-kaolinites which form directly by means of a layer-by-layer transformation. However, it is also conceivable that stripping of tetrahedral sheets as part of a layer-by-layer reaction mechanism could result in adjacent 1:1 layers with an interlayer containing hydrated exchangeable

cations (Cuadros and Dudek, 2006; Ryan and Huertas, 2009), and by most definitions, these layers would be termed halloysite (Churchman and Carr, 1975; Delvaux *et al.*, 1990b). Reaction of flaky K-S crystals to spheroids (or tubes) could occur if tetrahedral stripping caused layers to roll when halloysite layers are produced; this has been observed by Singh and Gilkes (1992). If this process results in K-S (H-S, technically) and is then followed by epitaxial crystallization of halloysite (with no interstratified smectite), it could explain HRTEM evidence for interstratified halloysite and smectite layers in the interiors of halloysite spheroids (Figure 9b).

Spheroidal halloysite appears earlier in the chronosequence than tubular halloysite, and the spheroidal halloysites are compositionally more similar to precursor smectite and K-S than are tubular halloysites (which have more-evolved Al-rich, Fe-poor compositions). Spheroidal halloysite tends to contain more Fe than tubular halloysite (Bailey, 1989; Soma *et al.*, 1992; Joussein *et al.*, 2005), a relationship which implies that spheroidal halloysite is altered to the tubular form with time (Sudo and Yotsumoto, 1977). The large difference in composition and morphology of spheroidal and tubular halloysite is more consistent with crystal dissolution-precipitation than a layer-by-layer mechanism for the spheroidal to tubular halloysite reaction. Berthonneau *et al.* (2015), however, suggested that tubular halloysite occurring in an altered rhyolite acts as a precursor template for growth of spheroidal halloysite, implying that reactions among these two halloysite types may not necessarily require dissolution and neoformation.

Differences in crystal morphology and the structure of kaolinite compared to halloysite (whether spheroidal or tubular) indicate that halloysite probably dissolves before crystallizing into fine-grained hexagonal kaolinite (in Qt1), a mechanism that has been demonstrated experimentally (La Iglesia and Galán, 1975), and one that is implied by the difference in layer stacking between kaolinite and halloysite. Kaolinite has a 1-layer structure whereas halloysite has a 2-layer repeat frequency (Bailey, 1989). These factors indicate that dissolution-precipitation rather than cell-preserved transformation occurs when spheroidal or tubular halloysites react to form hexagonal kaolinite (Wilson, 1999).

Diversity of 2:1 layers in smectite and K-S

In addition to kaolinite and smectite layer types, the phase termed K-S in the present study contains vermiculite-like 14 Å layers and illite-like 10 Å layers, and these layer types increase in abundance relative to Ca-smectite over time. Vermiculite-like layers are indicated in XRD results by incomplete collapse at 350ºC, evidence for which includes low-angle background and weak peaks in the 11−14 Å range, especially

in Qt2-150 (Figure 4a). Limited expansion with EG − especially in Qt2, the terrace soil with the greatest amount of K-S − is also observed in XRD analyses and can be modeled best using *NEWMOD* as an interstratified mineral containing dioctahedral vermiculite layers in addition to smectite layers and kaolinite layers. The vermiculite layers were included to represent 2:1 layers with Al-hydroxy interlayers, and they are needed to produce K-S 001 peaks in the 16 to 17.5 Å range; without 14 Å layers in addition to 17 and 7 Å layers, the K-S 001 peak occurs in the 18 to 22 Å range. The lack of measurable interlayer Ca^{2+} or K^+ in K-S from Qt2 and Qt1, as observed in TEM-AEM, is consistent with the presence of interlayer Al, but the continued capacity of interlayers to partially expand with EG is consistent with use of the term Al-hydroxy interlayer smectite (Meunier, 2007). The appearance of HIS layers over time is caused by the temporal evolution of the soil solution, *i.e.* increasing acidity and activity of Al and leaching loss of Ca^{2+} and K^+. Under these conditions, selective adsorption of species such as $[Al(OH)_2(H_2O)_4]^+$ in the interlayer tends to form incomplete gibbsite-like sheets with ~60% of the interlayer occupied by Al-hydroxy complexes (Meunier, 2007). The incomplete interlayer has been referred to as islands of positively charged Al-hydroxy complexes (Dixon and Jackson,1962; Barnhisel and Bertsch, 1989) that may allow cation exchange to occur between islands, especially if a 2:1 layer charge is not fully balanced by the Al-hydroxy complexes (Meunier, 2007).

Illite-like layers are indicated by a weak and broad 10 Å XRD peak in EG analyses, *e.g.* of Qt2-150 (Figure 4a), and the low intensity of this peak relative to 17 and 7 Å peaks indicates that illite-like layers are a minor component. Further support for the occurrence of this layer type is the presence of interlayer K^+ measured by TEM-AEM, notably in Qt-3 smectite. The K^+ detected by TEM-AEM is probably fixed in the interlayer space given that clays were saturated with Ca^{2+} prior to analysis, and the force retaining interlayer K^+ is probably due to individual layers or parts of layers where the negative charge is locally closer to an illite-like value, *e.g.* 0.7 mol_c p.f.u. rather than 0.3 or 0.4. In Qt4 smectites, interlayer Ca^{2+} is greater than interlayer K^+; in Qt3 smectites, interlayer K^+ is greater than interlayer Ca^{2+}. The retention of interlayer K^+ over Ca^{2+} in smectite interlayers as soils evolve has been observed previously and is related to a smaller hydration radius of K^+ relative to Ca^{2+} (Sawhney, 1972; Delvaux *et al.*, 1990a). Ca^{2+} is likely to be leached preferentially from the interlayer space and replaced by hydrated $Al(OH)_2^+$, especially within the first 50 ka of soil development when smectite and K-S are abundant phases. After this, the alteration of 2:1 layers to 1:1 layers is nearly complete, nearly all K^+ and Ca^{2+} have been leached from the soil, and Al occurring in hydroxy interlayers is reapportioned into aluminous octahedral sheets.

The term kaolinite-smectite (K-S), rather than K-I-V-S, for example, is used in the present study for these reasons: (1) kaolinite and smectite are the dominant layer types when modeled with *NEWMOD*; (2) the 2:1 layers with Al-hydroxy interlayers are comparable to hydroxy-interlayer smectite (HIS) (Meunier, 2007), so the term kaolinite-vermiculite-smectite (K-V-S) is less precise than K-S; (3) the illite-like layers appear to exert no strong influence on the XRD patterns of the interstratified clays, and while TEM-AEM indicates that K^+ (and possibly Al species) is more abundant than Ca^{2+} in interlayers of Qt3 flaky smectite-like crystals, this mineral expands to 16.2 Å, behavior which is consistent with partial expansion of smectite layers in HIS with localized K-rich and Al-hydroxy zones (Malla, 2002; Meunier, 2007); and (4) the most common term for this type of interstratified clay throughout the literature is kaolinite-smectite (*e.g.* Cradwick and Wilson, 1972; Herbillon *et al.*, 1981; Yerima *et al.*, 1985; Delvaux *et al.*, 1989; Righi *et al.*, 1999; Wilson, 1999; Dudek *et al.*, 2007; Cuadros *et al.*, 2009; Ryan and Huertas, 2009). At the same time, the precise identification and recognition of the complexity of soil K-S is important. When considering nutrient cycling, for example, smectite and interstratified K-S with illite-like layers or zones fosters retention of K^+ over Ca^{2+} (Delvaux *et al.*, 1990a), and the Al-hydroxy-interlayers of HIS may adsorb plant-toxic Al from soil and also retain space and charge for cation exchange (Meunier, 2007).

Morphology and composition of halloysite and kaolinite

Of the morphologies of halloysites described in the literature, a variety sometimes termed platy halloysite is the most Fe rich followed by spheroidal, then tubular habits (Noro, 1986; Soma *et al.*, 1992; Joussein *et al.*, 2005). In the present study, analysis by XRD and TEM documents the occurrence of Fe-kaolinite with ⩽10% smectite layers. The expandability of this phase detected by XRD might warrant the term platy halloysite (Kunze and Bradley, 1954; Bailey, 1989), but morphologically, compositionally, and structurally (*e.g.* HRTEM and XRD evidence of interstratified smectite layers), the more precise term is Fe-kaolinite (or K-S with ⩽10% smectite layers). Regardless of terminology, however, this appears to be the most Fe rich of soil kaolinites or halloysites, both in the present study and in the literature. The Nicoya sequence records progression from Fe-kaolinite to spheroidal halloysite, tubular halloysite, and then finally, platy hexagonal kaolinite, and this is also the progression from most Fe rich to most Al rich summarized by Joussein *et al.* (2005) and implied by thermodynamic considerations.

Chemically zoned spheroidal halloysites show a trend which at first is counter-intuitive – layers become progressively enriched in Fe and depleted in Al from core to rim. If spheroidal halloysites were to grow progressively over thousands or tens of thousands of years, crystals should have the opposite zoning because, over time, the soil clays in this sequence become depleted in Fe. Spheroidal halloysites were indicated by Tomura *et al.* (1985) to crystallize from supersaturated solutions. In tropical soils with pronounced rainy and dry seasons, like those in the present study, the transition from rainy to dry season drives the soil solutions toward supersaturation (Gloaguen *et al.*, 2007) and this favors kinetically the controlled formation of spheroidal halloysite (Zeigler *et al.*, 2003; Etame *et al.*, 2009). In the Nicoya chronosequence, spheroidal halloysite does not form until soils have weathered for 10 to 50 ka, but once leaching has sufficiently altered the system composition to an Al:Si ratio that favors crystallization of halloysite – and evaporation during the dry season drives up Si, Al, and Fe concentrations in the soil solution to saturation with respect to halloysite – crystals of spheroidal halloysite form, not slowly over millennia, but perhaps over days or months, an interpretation supported by synthesis experiments (Tsuzuki and Kawabe, 1983) and modeling with the code *NANOKIN* (Fritz *et al.*, 2009). Viewed in this way, the spheroidal halloysites in these samples are of different ages, formed during different dry seasons, and the most Fe-rich ones probably formed earlier than the Fe-poor ones. The source of octahedral Fe in spheroidal halloysite is mainly octahedral Fe inherited from precursor smectite layers. As smectite layers decrease in abundance over time, Fe in the clay assemblage decreases and becomes less available for incorporation into halloysites.

An additional thermodynamic consideration regarding zoning in crystals of spheroidal halloysites (*i.e.* the decrease in Al:Fe ratio from center to rim) is that the first layers of halloysite to crystallize when solutions reach saturation are predicted to be Al rich. Yet, as crystallization progresses (perhaps during a single dry season for a given crystal) and the Al:Fe ratio of the soil solution decreases, crystal growth produces layers with increasing octahedral Fe outward toward rims. This is evident in TEM-AEM data (Figure 8). Eventually, for some of the most Fe-rich halloysites, the abundance of available Fe relative to Al and Si reaches the point at which goethite forms on the surfaces of the spheroids.

Halloysites tend to have greater CEC than kaolinites (Delvaux *et al.*, 1992; Joussein *et al.*, 2005), an occurrence which has been attributed to layer charge caused either by isomorphous substitution (Mg^{2+} for Al^{3+} or Al^{3+} for Si^{4+}; McBride, 1976; Ma and Eggleton, 1999) or interstratification of smectite layers (Delvaux *et al.*, 1990b). Evidence for both is found in the Nicoya clays.

Implications for soil composition

Chemical compositions of pedogenic smectite in the Nicoya chronosequence are similar to ferruginous beidellites from other moist tropical soils (Kantor and Schwertman, 1974; Delvaux *et al.*, 1990b) and are very

similar to, but slightly more Si rich and Al poor than, pedogenic smectites from the slightly moister Esterillos region of Costa Rica (Ryan and Huertas, 2009). If only interlayer Ca^{2+} is exchangeable (*i.e.* K^+ and Al-hydroxy complexes are approximately fixed), average CEC based on TEM-AEM of Qt4 is 75 $cmol_c/kg$ (range = 51−97 $cmol_c/kg$), a value that compares well with a 71.3 $cmol_c/kg$ CEC average (range = 48−89 $cmol_c/kg$) for a larger suite of samples from the study area determined by NH_4OAc analysis (Pincus, 2014). Similar CEC values have been measured for pedogenic smectites from tropical soils (Kantor and Schwertman, 1974; Pincus, 2014) and from Mediterranean soils (67−72 $cmol_c/kg$; Righi *et al.*, 1998). According to compositional analysis of NH_4OAc-extracted solutions, Ca^{2+} is the dominant exchangeable cation in the Nicoya smectites (Pincus, 2014).

Compared to Holocene-age tropical soils rich in smectite and K-S, Pleistocene tropical soils with abundant halloysite and kaolinite tend to have poorer nutrient-retention capability, lower bulk density, greater hydraulic conductivity, and lower available water capacity (Minasny and Hartemink, 2011). Decreasing abundance of plant nutrients caused by chemical leaching occurs simultaneously with the sequential reaction of smectite to K-S, halloysite, and kaolinite in these soils, *i.e.* from high-activity smectites with CEC of 50−85 $cmol_c/kg$ (Pincus, 2014) to low-activity clays (halloysites, kaolinites) with CEC of 11−16 $cmol_c/kg$. The Nicoya chronosequence dataset includes − among the plant nutrients − K^+, Ca^{2+}, Mg^{2+}, and PO_4^{3-} (Table 2); of these, K^+ and Ca^{2+} are leached most rapidly and after 120 ka of soil formation, reach bulk-soil concentrations of $\leqslant 0.4\%$ (Ca) and $\leqslant 0.1\%$ (K). Factors responsible for this are: (1) the tendency of K^+ and Ca^{2+} to enter the aqueous solution when released by mineral weathering, enhancing potential to be leached out of soil; (2) conversion of smectite to kaolinite, a progression which results in loss of negative layer charge and interlayer space to retain cations; and (3) exchange reactions driven by low pH and high activity of Al in solution, *i.e.* as primary minerals are exhausted and pH decreases with time, Al activity in soil solution increases and Al becomes incorporated into interlayers (as Al-hydroxy complexes) and K^+ and Ca^{2+} are released to solution to be leached out of soil. Mg^{2+} often is as soluble as K^+ and Ca^{2+} but, unlike these large cations (which only fit into interlayers in clays), Mg^{2+} is incorporated into octahedral sheets when smectite forms, and thus is less available for leaching from soil than the interlayer cations; later, when smectite layers are altered to 1:1 layers in K-S or halloysite, Mg^{2+} is released to solution

Retention of K^+ and (to a lesser extent) Ca^{2+} by intermediate-stage K-S is demonstrated by TEM-AEM single-crystal measurements which indicate the presence of K^+ and Ca^{2+} in interlayers (Tables 3, 4). On a molar basis, K-S-bearing Qt2 soil (50 ka) contains twice as much K^+ and Ca^{2+} as 120 ka Qt1 soil, and its CEC (28 $cmol_c/kg$) is intermediate between that of smectite and the 1:1 clays. K-S is more abundant in Qt2 than in Qt1 and it contains a greater abundance of smectite layers (10−40%) than does Qt1 K-S (<10% smectite layers) and the greater nutrient content and higher CEC is attributed to greater abundance of smectite interlayers. An additional benefit provided to soil by K-S is the ability to incorporate plant-toxic Al into smectite interlayers (Korning *et al.*, 1994; Ndayiragije and Delvaux, 2003; Ryan and Huertas, 2009). The 11−16 $cmol_c/kg$ CEC of Qt1 clay (halloysite + kaolinite) is typical of low-activity clays observed in many evolved tropical soils (*e.g.* Anjos *et al.*, 1998; Hart *et al.*, 2002; Ndayiragije and Delvaux, 2003; Pochet *et al.*, 2007; Hughes *et al.*, 2009). The CEC of these clays may be greater than reference kaolinites with values of 3−4 $cmol_c/kg$ because of negative charge on the 1:1 layer imparted by residual Mg^{2+} and by non-stoichiometric substitution of Fe for Al (Soma *et al.*, 1992).

Global significance of time-dependent mineralogy of tropical soil

Research shows that tropical soils are diverse, spanning a wide range of age, composition, and structure (Vitousek and Sanford, 1986; Tardy and Roquin, 1992; Minasny and Hartemink, 2011). The paradigmatic, extensively leached, acidic, base-poor, Al-rich, and kaolinite-dominated tropical soil, *i.e.* Oxisol or Ultisol, occurs in 43% of the tropics (Szott *et al.*, 1991); the remainder are either too young to have evolved into Oxisols or Ultisols, or occur in climates with insufficient rainfall to form Oxisols or Ultisols. Globally, Inceptisols and Entisols account for 31% of tropical soils (Szott *et al.*, 1991), and compositionally they represent the early stages in the alteration of parent material. As is illustrated by the Holocene soils of the Nicoya chronosequence, they are rich in smectite or K-S and, depending on abundance of rainfall, require time scales on the order of 10^4 to 10^5 y to undergo alteration to halloysite and/or kaolinite.

In tectonically active, moist, tropical regions, where volcanism, uplift, and erosion expose fresh parent materials, Oxisols are notably rare; *e.g.* in Costa Rica, Oxisols are <1% of all soils, and Inceptisols (40%) are the most common soil order (Mata, 1991). From the relatively dry Nicoya Peninsula (1600−3200 mm/y MAP) to the very rainy Osa Peninsula (4000−5000 mm/y MAP), Holocene terrace soils are dominated by smectite and Late Pleistocene soils are dominated by K-S, halloysite, and kaolinite (Fisher and Ryan, 2006; Ryan and Huertas, 2009; Pincus, 2014). In Papua, Oxisols constitute <1% and Inceptisols constitute 48% of soils (Hope and Hartemink, 2007). Inceptisol−Oxisol transitions occur in Nicaragua (Eswaran and DeConinck, 1971), and Hawaii is well

known for variability in soil composition caused in part by age differences, and also by climate and parent-material variability (Stewart *et al.*, 2001; Zeigler *et al.*, 2003). In tectonically active tropical landscapes, periodic exposure of unweathered parent material starts the soil-forming process anew, meaning that soils in these regions will range from early-stage smectite-dominated, high-CEC, approximately neutral pH, and base cation-rich to intermediate K-S and halloysite to eventually evolved, base cation-depleted, low-CEC, low pH, kaolinite-rich Oxisols (eventually with gibbsite in some very high-rainfall environments). Analysis of age-related clay-mineral reaction sequences from dry to very moist tropical climate regimes, and in tropical soils with different parent materials, will provide the additional data needed to develop a comprehensive predictive tool for soil composition both spatially and temporally.

CONCLUSIONS

Halloysite and kaolinite in lateritic Alfisols of a soil chronosequence in northwestern Costa Rica originated as smectite that forms in the earliest stage of pedogenesis in this moist tropical environment. The sequence can be summarized as follows:

(1) In young soils ($\leqslant 8$ ka), Fe-rich smectite is the only pedogenic mineral detected other than trace amounts of incipient K-S. The smectites have high CEC (50$-$85 cmol$_c$/kg) and are associated with circum-neutral soil pH (6.1$-$7.4) and (in some cases) poor drainage.

(2) After 10$-$50 ka of pedogenesis, interstratified K-S and Fe-rich spheroidal halloysite are the dominant soil minerals; the K-S $-$ which contains interlayers of readily exchangeable Ca^{2+} and relatively-fixed K^+ and Al-hydroxy complexes $-$ forms by lateral transformation of smectite layers within crystallites, whereas the halloysite probably crystallizes by neoformation after dissolution of precursor K-S or smectite. These intermediate-age soils appear lateritic in the field and have low pH (5.1$-$5.3) but intermediate CEC (18 to 28 cmol$_c$/kg), an attribute caused by residual smectite layers in K-S; spheroidal halloysite may also contribute to the CEC by means of substitution of Mg^{2+} and Fe^{3+} for Al^{3+} (octahedral) and Al^{3+} for Si^{4+} (tetrahedral) which result in negative layer charge and site vacancies.

(3) After 120 ka of pedogenesis, soil is dominated by 1:1 clays including (in order of decreasing abundance): Fe-kaolinite (some containing residual smectite layers [<10%]) > halloysite (both spheroidal and tubular) > hexagonal crystals of low-Fe kaolinite. The halloysite+kaolinite assemblage has a small CEC value (11$-$16 cmol$_c$/kg) and soils have low reserves of base cations. They are also moderately acidic (pH of 4.7$-$5.3).

(4) The smectite $\rightarrow$ K-S $\rightarrow$ halloysite to kaolinite sequence observed in the Nicoya chronosequence is

expected based on thermodynamic considerations that apply to a system undergoing leaching of Si and base cations. Smectite is kinetically favored by short-lived conditions of high Si and base cations in soil solution provided by rapidly dissolving primary minerals. 120 ka of leaching has increased the molar Al:Si ratio of bulk soil from 0.3 (Qt4) to 0.8 (Qt1), a value approaching the Al:Si ratio of 1:1 that favors the formation and persistence of halloysite or kaolinite. The prograde, age-driven control on the composition of moist tropical soils has been observed elsewhere in Central and South America as well as in moist tropical soils of Africa and southeast Asia; it is a model that is especially applicable to landscapes where active uplift, volcanic activity, erosion, or deposition periodically expose unweathered parent material at the surface and result in soils of varied ages.

REFERENCES

Abayneh, E., Zauyah, S., Hanafi, M.M., and Rosenani, A.B. (2006) Genesis and classification of sesquioxidic soils from volcanic rocks in sub-humid tropical highlands of Ethiopia. *Geoderma*, **136**, 682$-$695

Albertin, W. (1962) *The Southern Tip of the Nicoya Peninsula*. Instituto Interamericano de Ciencias Agricolas, Turrialba, Costa Rica, 59 pp.

Alexander, E.B. and Holowaychuk, N. (1983) Soils on terraces along the Cauca River, Colombia. II. The sand and clay fractions. *Soil Science Society of America Journal*, **47**, 721$-$727.

Amouric, M. and Olives, J. (1998) Transformation mechanisms and interstratification in conversion of smectite to kaolinite; an HRTEM study. *Clays and Clay Minerals*, **46**, 521$-$527.

Anderson, R.S., Densmore, A.L., and Ellis, M.A. (1999) The generation and degradation of marine terraces. *Basin Research*, **11**, 7$-$19.

Anjos, L.H. Fernandas, M.R., Pereira, M.G., and Franzmeier, D.P. (1998) Landscape and pedogenesis of an Oxisol-Inceptisol-Ultisol sequence in Southeastern Brazil. *Soil Science Society of America Journal*, **62**, 1651$-$1658.

Askenasy, P.E., Dixon, J.B., and McKee, T.R. (1973) Spheroidal halloysite in a Guatemalan soil: *Soil Science Society of America Proceedings*, **37**, 799$-$803.

Bailey, S.W. (1989) Halloysite $-$ a critical assessment. Proceedings of the International Clay Conference, Strasbourg, France. *Scientifique Geologie Memoires*, **86**, 89$-$98.

Balan, E., Allard, T., Boizot, B., Morin, G., and Muller, A.P. (1999) Structural Fe^{3+} in natural kaolinites: new insights from EPR spectra fitting at X- and Q-band frequencies.

Clays and Clay Minerals, **47**, 605−616.

Balan, E., Fritsch, E., Allard, T., and Calas, G. (2007) Inheritance *vs.* neoformation of kaolinite during lateritic soil formation: a case study in the middle Amazon. *Clays and Clay Minerals*, **55**, 253−259.

Barnhisel, R.I. and Bertsch, P.M. (1989) Chlorites and hydroxy-interlayered vermiculite and smectite. Pp. 729−788 in: *Minerals in Soil Environments*, 2nd edition (J.B. Dixon and S.B. Weed, editors). Soil Science Society of America, Madison, Wisconsin, USA.

Berthonneau, J., Grauby, O., Jeannin, C., Chaudanson, D., Joussein, E., and Baronnet, A. (2015) Native morphology of hydrated spheroidal halloysite observed by environmental transmission electron microscopy. *Clays and Clay Minerals*, **63**, 368−377.

Birkeland, P.W. (1999) *Soils and Geomorphology*. Oxford University Press, Oxford, UK.

Black, C.A. (1965) *Methods of Soil Analysis: Part 2, Chemical and Microbiological Properties.* American Society of Agronomy, Madison, Wisconsin USA.

Borden, D. and Giese, R.F. (2001) Baseline studies of the Clay Minerals Society source clays: cation exchange capacity measurements by the ammonia−electrode method. *Clays and Clay Minerals*, **49**, 444−445.

Bravard, S. and Righi, D. (1988) Characteristics of clays in an Oxisol−Spodosol toposequence in Amazonia (Brazil). *Clay Minerals*, **23**, 279−289.

Brindley, G.W. (1961) Kaolin, serpentine and kindred minerals. Pp. 51−131 in: *The X-ray Identification and Crystal Structures of Clay Minerals* (G. Brown, editor). Mineralogical Society, London.

Bühmann, C. and Grubb, P.L.C. (1991) A kaolin-smectite interstratification sequence from a red and black complex. *Clay Minerals*, **26**, 343−358.

Calvert, C.S., Buol, S.W., and Weed, S.B. (1980) Mineralogical characteristics and transformations of a vertical-rock-saprolite-soil sequence in the North Carolina Piedmont: II. Feldspar alteration products − their transformations through the profile. *Soil Science Society of America Journal*, **44**, 1104−1112.

Churchman, G.J. and Carr, R.M. (1975) The definition and nomenclature of halloysites. *Clays and Clay Minerals*, **23**, 382−388.

Churchman, G.J. and Gilkes, R.J. (1989) Recognition of intermediates in the possible transformation of halloysite to kaolinite in weathering profiles. *Clay Minerals*, **24**, 579−590.

Churchman, G.J., Slade, P.G., Self, P.G., and Janik, L.J. (1994) Nature of interstratified kaolin-smectites in some Australian soils. *Australian Journal of Soil Research*, **32**, 805−822.

Cliff, G. and Lorimer, G.W. (1975) The quantitative analysis of thin specimens. *Journal of Microscopy*, **103**, 203−207.

Cradwick, P.D. and Wilson, M.J. (1972) Calculated X-ray diffraction profiles for interstratified kaolinite-montmorillonite. *Clay Minerals*, **9**, 395−405.

Cuadros, J. and Dudek, T. (2006) FTIR investigation of the evolution of the octahedral sheet of kaolinite-smectite with progressive kaolinization. *Clays and Clay Minerals*, **54**, 1−11.

Cuadros, J., Delgado, A., Cardenete, A., Reyes, E., and Linares, J. (1994) Kaolinite/montmorillonite resembles smectite. *Clays and Clay Minerals*, **42**, 643−651.

Cuadros, J., Nieto, F., and Wing-Dudek, T. (2009) Crystal-chemical changes of kaolinite-smectite mixed-layer with progressive kaolinization, as investigated by TEM-AEM and HRTEM. *Clays and Clay Minerals*, **57**, 742−750.

de Ligny, D. and Navrotsky, A. (1999) Energetics of kaolin polymorphs. *American Mineralogist*, **84**, 506−516.

de Oliveira, M.T.G., Petit, S., Grauby, O., Formoso, M.L.L., and Trescases, J.J. (1997) Characterization and distribution of halloysitic clay minerals in weathered basalts (southern Parana Basin, Brazil). *Anais-Academia Brasileira de Ciencias*, **69**, 179−192.

Dean, J.A. (1979) *Lange's Handbook of Chemistry*, 12th edition, McGraw-Hill, New York.

Delvaux, B., Mestdagh, M.M., Vielvoye, L., and Herbillon, A.J. (1989) XRD, IR and ESR study of experimental alteration of Al-nontronite into mixed-layer kaolinite-smectite. *Clay Minerals*, **24**, 617−630.

Delvaux, B., Herbillon, A.J., Dufey, J.E., and Vielvoye, L. (1990a) Surface properties and clay mineralogy of hydrated halloysitic soil clays. I: Existence of interlayer K^+ specific sites. *Clay Minerals*, **25**, 129−139.

Delvaux, B., Herbillon, A.J., Vielvoye, L., and Mestdagh, M.M. (1990b) Surface properties of clay mineralogy of hydrated halloysitic soil clays. II: Evidence for the presence of halloysite/smectite (H/Sm) mixed-layer clays. *Clay Minerals*, **25**, 141−160.

Delvaux, B., Tessier, D., Herbillon, A.J., and Burtin, G. (1992) Morphology, texture, and microstructure of halloysitic soil clays as related to weathering and exchangeable cation. *Clays and Clay Minerals*, **40**, 446−45.

Delvaux, B. and Herbillon, A.J. (1995) Pathways of mixed-layer kaolin-smectite formation in soils. Pp. 457−461 in: *Clays Controlling the Environment* (G.J. Churchman, R.W. Fitzpatrick, and R.A. Eggleton, editors). Proceedings of the 10th International Clay Conference, Adelaide, Australia.

Dixon, J.B. and Jackson, M.L. (1962) Properties of inter-gradient chlorite-expansible layer silicates of soils. *Soil Science Society of America Proceedings*, **26**, 358−362.

Dohrmann, R. (2006) Problems in CEC determination of calcareous clayey sediments using the ammonium acetate method. *Journal of Plant Nutrition and Soil Science*, **169**, 330−334.

Dudek, T., Cuadros, J., and Fiore, S. (2006) Interstratified kaolinite-smectite: nature of the layers and mechanism of smectite kaolinization. *American Mineralogist*, **91**, 159−170.

Dudek, T., Cuadros, J., and Huertas, F.J. (2007) Structure of mixed-layer kaolinite-smectite and smectite-to-kaolinite transformation mechanism from synthesis experiments. *American Mineralogist*, **92**, 179−192.

Eswaran, H. and De Coninck, F. (1971) Clay mineral formations and transformations in basaltic soils in tropical environments. *Pedologie*, **21**, 181−210.

Eswaran, H. and Wong, C.B. (1978) A study of a deep weathering profile on granite in peninsular Malaysia: III. Alteration of feldspars. *Soil Science Society of America Journal*, **42**, 154 −158.

Eswaran, H., Beinroth, F.H., Kimble, J., and Cook, T. (1992) Soil diversity in the tropics: implications for agricultural development. Pp. 1−16 in: *Myths and Science of Soils of the Tropics* (R. Lal and P.A. Sanchez, editors). Special Publication **29**, Soil Science Society of America, Madison, Wisconsin, USA.

Etame, J., Gerard, M., Suh, C.E., and Bilong, P. (2009) Halloysite neoformation during the weathering of nephelinitic rocks under humid tropical conditions at Mt Etinde, Cameroon. *Geoderma*, **154**, 59−68.

Fisher, G.B. and Ryan, P.C. (2006) The smectite to disordered kaolinite transition in a tropical soil chronosequence, Pacific Coast, Costa Rica. *Clays and Clay Minerals*, **54**, 571−586.

Fritz, B., Clement, A., Amal, Y., and Noguera, C. (2009) Simulation of nucleation and growth of simple clay minerals in weathering processes: The NANOKIN code. *Geochimica et Cosmochimica Acta*, **73**, 1340−1358.

Gaudin, A., Petit, S., Rose, J., Martin, F., Decarreau, A., Noack, Y., and Borschneck, D. (2004) The accurate crystal

chemistry of ferric smectites from the lateritic nickel ore of Murrin Murrin (Western Australia). II. Spectroscopic (IR and EXAFS) approaches. *Clay Minerals*, **39**, 453−467.

Geldmacher, J., Hoernle, K., van den Bogaard, P., Hauff, F., and Klügel, A. (2008) Age and geochemistry of the Central American forearc basement (DSDP Leg 67 and 84): Insights into Mesozoic arc volcanism and seamount accretion on the fringe of the Caribbean LIP. *Journal of Petrology*, **49**, 1781−1815.

Gloaguen, T.V., Forti, M.C., Lucas, Y., Montes, C.R., Gonçalves, R.A.B., Herpin, U., and Melfi, A.J. (2007) Soil solution chemistry of a Brazilian Oxisol irrigated with treated sewage effluent. *Agricultral Water Management*, **88**, 119−131.

Gracheva, R.G., Targulian, V.O., and Zamotaev, I.V. (2001) Time-dependent factors of soil and weathering mantle diversity in the humid tropics and subtropics: a concept of soil self-development and denudation. *Quaternary International*, **78**, 3−10.

Greene, A.M., Seager, R., and Broecker, W.S. (2002) Tropical snowline depression at the Last Glacial Maximum: comparison with proxy records using a single-cell tropical climate model. *Journal of Geophysical Research*, **107**, DOI: 10.1029/2001JD000670.

Grim, R.E. (1968) *Clay Mineralogy*. McGraw-Hill, New York, 596 pp.

Hart, R.D., Gilkes, R.J., Siradz, S., and Singh, B. (2002) The nature of soil kaolins from Indonesia and western Australia. *Clays and Clay Minerals*, **50**, 198−207.

Harward, M.E., Carstea, D.D., and Sayegh, A.H. (1969) Properties of vermiculites and smectites: expansion and collapse: *Clays and Clay Minerals*, **16**, 437−447.

He, Y., Li, D.C., Velde, B., Yang, Y.F., Huang, C.M., Gong, Z.T., and Zhang, G.L. (2008) Clay minerals in a soil chronosequence derived from basalt on Hainan Island, China and its implication for pedogenesis. *Geoderma*, **148**, 206−212.

Herbillon, A.J., Mestdagh, M.M., Vielvoye, L., and Derouane, E.G. (1976) Iron in kaolinite with special reference to kaolinite from tropical soils. *Clay Minerals*, **11**, 201−220.

Herbillon, A.J., Frankart, R., and Vielvoye, L., (1981) An occurrence of interstratified kaolinite-smectite minerals in a red-black soil toposequence. *Clay Minerals*, **16**, 195−201.

Hillier, S. and Ryan, P.C. (2002) Identification of halloysite (7 Å) by ethylene glycol solvation: the 'MacEwan effect.' *Clay Minerals*, **37**, 487−496.

Hobbs, F.W.C. (2012) Smectite-to-disordered kaolinite transitions as a function of age in the Nicoya Peninsula. Unpublished Bachelor's thesis, Middlebury College, Middlebury, Vermont, USA, 61 pp. http://middarchive.mid-dlebury.edu/cdm/search/collection/scholarship!scholrestrct/searchterm/*!geology/

Hope, G.S. and Hartemink A.E. (2007) Soils of Papua. Pp. 165−176 in: *The Ecology of Papua* (A.J. Marshall and B.M. Beehler, editors). Periplus Editions, Singapore.

Hughes, J.C. (1980) Crystallinity of kaolin minerals and their weathering sequence in some soils from Nigeria, Brazil, and Colombia. *Geoderma*, **24**, 317 − 325.

Hughes, J.C., Gilkes, R.J., and Hart, R.D. (2009) Intercalation of reference and soil kaolins in relation to physico-chemical and structural properties. *Applied Clay Science*, **45**, 25−35.

Hughes, R.E., Moore, D.M., and Reynolds, R.C., Jr. (1993) The nature, detection and occurrence, and origin of kaolinite/smectite. Pp. 291−323 in: *Kaolin Genesis and Utilization* (H.H. Murray, W.M. Bundy, and C.C. Harvey, editors), Special Publication No. **1**, The Clay Minerals Society, Boulder, Colorado, USA.

Instituto Meteorológico Nacional (IMN) de Costa Rica, *Atlas Climatológico*. [https://www.imn.ac.cr/39]. Accessed 21 April 2016.

Iriarte, I., Petit, S., Huertas, F.J., Fiore, S., Grauby, O., Decarreau, A., and Linares, J. (2005) Synthesis of kaolinite with a high level of Fe^{3+} for Al substitution. *Clays and Clay Minerals*, **53**, 1−10.

Jiang, J., Xu, R., and Zhao, A. (2011) Surface chemical properties and pedogenesis of tropical soils derived from basalts with different ages in Hainan, China. *Catena*, **87**, 334−340.

Joussein, E., Petit, S., Churchman, J., Theng, B., Righi, D., and Delvaux, B. (2005) Halloysite clay minerals − a review. *Clay Minerals*, **40**, 383−426.

Kantor, W. and Schwertmann, U. (1974) Mineralogy and genesis of clays in red-black toposequences in Kenya. *Journal of Soil Science*, **25**, 67−78.

Kautz, C.Q. and Ryan, P.C. (2003) The 10 Å to 7 Å halloysite transition in a tropical soil sequence, Costa Rica. *Clays and Clay Minerals*, **51**, 252−263.

Karathanasis, A.D. and Hajek, B.F. (1984) Evaluation of Al-smectite stability of equilibria in naturally acid soils. *Soil Science Society of America Journal*, **48**, 413−417.

Keller, W.D. (1977) Scan electron micrographs of kaolins collected from diverse environments of origin − IV. Georgia kaolin and kaolinizing source rocks: *Clays and Clay Minerals*, **25**, 311−345.

Korning, J., Thomsen, K., Dalsgaard, K., and Nørnberg, P. (1994) Characters of three udults and their relevance to the composition and structure of virgin rain forest of Amazonian Ecuador. *Geoderma*, **63**, 145−164.

Kunze, G.W. and Bradley, W.F. (1954) Occurrence of a tabular halloysite in a Texas soil. *Clays and Clay Minerals*, **12**, 523−527.

La Iglesia, A. and Galán, E. (1975) Halloysite-kaolinite transformation at room temperature. *Clays and Clay Minerals*, **23**, 109−113.

Lal, R. (1995) *Sustainable Management of Soil Resources in the Humid Tropics*. United Nations University Press, Tokyo.

Lundberg, N. (1991) Detrital record of the early Central American magmatic arc: petrography of intraoceanic forearc sandstones, Nicoya Peninsula, Costa Rica. *Geological Society of America Bulletin*, **103**, 905−915.

Ma, C. and Eggleton, R.A. (1999) Cation exchange capacity of kaolinite. *Clays and Clay Minerals* **47**, 174−180.

MacEwan, D.M.C. (1948) Complexes of clays with organic compounds. I. Complex formation between montmorillonite and halloysite and certain organic liquids. *Transactions of the Faraday Society*, **44**, 349−367.

Madeira, M., Auxtero, E., and Sousa, E. (2003) Cation and anion exchange properties of Andisols from the Azores, Portugal, as determined by the compulsive exchange and the ammonium acetate method. *Geoderma*, **117**, 225−241.

Malla, P.B. (2002) Vermiculites. Pp. 501−529 in: *Soil Mineralogy with Environmental Applications*. (J.B. Dixon, and D.G. Schulze, editors). Soil Science Society of America, Madison, Wisconsin, USA.

Marshall, J.S. and Anderson, R.S. (1995) Quaternary uplift and seismic cycle deformation, Nicoya Peninsula, Costa Rica. *Geological Society of America Bulletin*, **107**, 463−473.

Marshall, J.S., LaFromboise, E.J., Gardner, T.W., and Protti, M. (2007) Segmented forearc deformation along the Nicoya Peninsula seismic gap, Costa Rica. *Eos, Transactions of the American Geophysical Union*, **88**, Fall Meeting Supplement, Abs T53A-1121.

Marshall, J.S., Morrish, S., LaFromboise, E., Butcher, A., Ritzinger, B., Wellington, K., Barnhart, A., Kinder, K., Utick, J., Protti, M., Gardner, T., Fisher, D., Simila, G., Spotila, J., Owen, L., Murari, M., and Cupper, M. (2012) Morphotectonic segmentation along the Nicoya Peninsula seismic gap, Costa Rica, Central America. *Seismological*

Research Letters, **83**, 374.

Mata, R. (1991) *Los ordenes de suelos de Costa Rica. Taller de Erosión*. Memoria, Heredia, MADE, UNA, Costa Rica.

McBride, M.B. (1976) Origin and position of exchange sites in kaolinite: As ESR study. *Clays and Clay Minerals*, **24**, 88–92.

Meunier, A. (2007) Soil hydroxy-interlayered minerals: A re-interpretation of their crystallochemical properties. *Clays and Clay Minerals*, **55**, 380–388.

Minasny, B. and Hartemink, A.E. (2011) Predicting soil properties in the tropics. *Earth-Science Reviews*, **106**, 52–62.

Moore, D.M. and Reynolds, R.C. Jr. (1997) Identification of mixed-layer minerals. Pp. 261–297 in: *X-ray Diffraction and the Identification and Analysis of Clay Minerals*. Oxford University Press, New York.

Nahon, D.B. and Colin, F. (1982) Chemical weathering of orthopyroxenes under lateritic conditions. *American Journal of Science*, **282**, 1232–1243.

Navarrete, I.A., Tsutsuki, K., Asio, V.B., and Kondo, R. (2009) Characteristics and formation of rain forest soils derived from late Quaternary basaltic rocks in Leyte, Philippines. *Environmental Geology*, **58**, 1257–1268. doi: 10.1007/s00254-008-1627-z.

Ndayiragije, S. and Delvaux, B. (2003) Coexistence of allophone, gibbsite, kaolinite and hydroxy-Al-interlayered 2:1 clay minerals in a perudic Andosol. *Geoderma*, **117**, 203–214.

Newman, A.C.D. and Brown, G. (1987) The chemical constitution of clays. Pp. 1–128 in: *Chemistry of Clays and Clay Minerals* (A.C.D. Newman, editor). Monograph, **6**, Mineralogical Society, Longman Technical and Scientific, Harlow, Essex, UK.

Nieuwenhuyse, A., Verburg, P.S.J., and Jongmans, A.G. (2000) Mineralogy of a soil chronosequence on andesitic lava in humid tropical Costa Rica. *Geoderma*, **98**, 61–82.

Noro, H. (1986) Hexagonal platy halloysite in an altered tuff bed, Komaki city, Aichi prefecture, central Japan. *Clay Minerals*, **21**, 401–415.

Parham, W.E. (1969) Formation of halloysite from feldspar: low temperature, artificial weathering versus natural weathering. *Clays and Clay Minerals*, **17**, 13–22.

Patino, L.C., Alvarado, G.E., and Vogel, T.A. (2004) Early arc magmatism: geochemical characteristics of volcanic clasts from Punta Sámara, Costa Rica. *Revista Geológica de América Central*, **30**, 117–125

Petit, S. and Decarreau, A. (1990) Hydrothermal (200ºC) synthesis and crystal chemistry of iron-rich kaolinites. *Clay Minerals*, **25**, 181–196.

Pincus, L. (2014) Variations in cation exchange capacity of clay soils across a tropical landscape. Unpublished Bachelor's thesis, Middlebury College, Middlebury, Vermont, 117 pp. http://middarchive.middlebury.edu/cdm/search/collection/scholarship!scholrestrct/searchterm/*!geology/

Piperno, D.R. and Jones, J.G. (2003) Paleoecological and archaeological implications of a Late Pleistocene/Early Holocene record of vegetation and climate from the Pacific coastal plain of Panama. *Quaternary Research*, **59**, 79–87.

Pochet, G., Van der Velde, M., Vanclooster, M., and Delvaux, B. (2007) Hydric properties of high charge, halloysitic clay soils from the tropical South Pacific region. *Geoderma*, **138**, 96–109.

Reheis, M.C. (1987) Gypsic soils on the Kane alluvial fans, Big Horn County, Wyoming. *U.S. Geological Survey Bulletin*, 1590-C, 39 pp.

Reynolds, R.C. III (2012) NEWMOD II for Windows ©. http://www.newmod-for-clays.com/

Righi, D., Terribile, F., and Petit, S. (1998) Pedogenic formation of high-charge beidellite in a Vertisol of Sardinia (Italy) *Clays and Clay Minerals*, **46**, 167–177.

Righi, D., Terribile, F., and Petit, S. (1999) Pedogenic formation of kaolinite-smectite mixed layers in a soil toposequence developed from basaltic parent material in Sardinia (Italy). *Clays and Clay Minerals*, **47**, 505–514.

Robertson, I.D.M. and Eggleton, R.A. (1991) Weathering of granitic muscovite to kaolinite and halloysite and of plagioclase-derived kaolinite to halloysite. *Clays and Clay Minerals*, **39**, 113–126.

Russell, J.D. and Fraser, A.R. (1994) Infrared methods. Pp. 11–67 in: *Clay Mineralogy: Spectroscopic and Chemical Determinative Methods* (M.J. Wilson, editor). Chapman & Hall, London.

Ryan P.C. and Huertas, F.J. (2009) The temporal evolution of pedogenic Fe-smectite to Fe-kaolin via interstratified kaolin-smectite in a moist tropical soil chronosequence. *Geoderma*, **151**, 1–15.

Ryan P.C. and Huertas, F.J. (2013) Reaction pathways of clay minerals in tropical soils: insights from kaolinite-smectite synthesis experiments. *Clays and Clay Minerals*, **61**, 303–318.

Sak, P.B., Fisher, D.M., Gardner, T.W., Marshall, J.S., and LaFemina, P.C. (2009) Rough crust subduction, fore arc kinematics, and Quaternary uplift rates, Costa Rican segment of the Middle American Trench. *Geological Society of America Bulletin*, **121**, 992–1012.

Sawhney, B.L. (1972) Selective sorption and fixation of cations by clay minerals: A review. *Clays and Clay Minerals*, **20**, 93–100.

Schaefer, C.E.G.R., Fabris, J.D., and Ker, J.C. (1988) Minerals in the clay fraction of Brazilian Latosols (Oxisols): a review. *Clay Minerals*, **43**, 137–154.

Schulze, D.G. (2005) *Clay Minerals*. Pp. 246–254 in: *Encyclopedia of Soils in the Environment*, Vol. 1 (D. Hillel, editor-in-chief). Elsevier Academic Press, Boston, Massachusetts, USA.

Selvaradjou, S.-K., Montanarella, L., Spaargaren, O., and Dent, D. (2005) *European Digital Archive of Soil Maps (EuDASM) - Soil Maps of Latin America and Carribean Islands* (DVD-Rom version). EUR 21822 EN. Office of the Official Publications of the European Communities, Luxembourg. http://eusoils.jrc.ec.europa.eu/Esdb_Archive/EuDASM/indexes/pubs.htm ; accessed 29-November 2016.

Shainberg, I., Alperovitch, N.I., and Keren, R. (1987) Charge density and Na-K-Ca exchange on smectites. *Clays and Clay Minerals*, **35**, 68–73.

Silva, A.C., Bispo, F.H.A., de Souza, S., Ardisson, J.D., Viana, A.J.S., Pereira, M.C., Costa, F.R., Murad, E., and Fabris, J.D. (2013) Iron mineralogy of a grey Oxisol from the Jequitinhonha River Basin, Minas Gerais, Brazil. *Clay Minerals*, **48**, 713–723.

Singh, B. and Gilkes, R.J. (1992) Properties of soil kaolinites from south-western Australia. *Journal of Soil Science*, **43**, 645–667.

Singh, B. and Gilkes, R.J. (1993) Weathering of spodumene to smectite in a lateritic environment. *Clays and Clay Minerals*, **41**, 624–630.

Soma, M., Churchman, G.J., and Theng, B.K.G. (1992) X-ray photoelectron spectroscopic analysis of halloysites with different composition and particle morphology. *Clay Minerals*, **27**, 413–421.

Środoń, J. (1999) Nature of mixed-layer clays and mechanisms of their formation and alteration. *Annual Review of Earth and Planetary Sciences*, **27**, 19–53.

Stevens, P.R. and Walker, T.W. (1970) The chronosequence concept and soil formation. *The Quarterly Review of Biology*, **45**, 333–350.

Stewart, B.W., Capo, R.C., and Chadwick, O.A. (2001) Effects of rainfall on weathering rate, base cation provenance, and Sr isotope composition of Hawaiian soils. *Geochimica et Cosmochimica Acta*, **65**, 1087−1099.

Sudo, T. and Yotsumoto, H. (1977) The formation of halloysite tubes from spherulitic halloysite. *Clays and Clay Minerals*, **25**, 155−159.

Szott, L.T., Palm, C.A., and Sanchez, P.A. (1991) Agroforestry in acid soils in the humid tropics. *Advances in Agronomy*, **45**, 275−301.

Szymanski, D.W., Patino, L.C., Vogel, T.A., and Alvarado, G.E. (2013) Evaluating complex magma mixing via polytopic vector analysis (PVA) in the Papagayo Tuff, northern Costa Rica: Processes that form continental crust. *Geosciences*, **3**, 585−615.

Tardy, Y. and Roquin, C. (1992) Geochemistry and evolution of lateritic landscapes. Pp. 407−443 in: *Developments in Earth Surface Processes* (I.P. Martini and W. Chesworth, editors). Elsevier, Amsterdam.

Thomas, G.W. (1996) Soil pH and soil acidity. Pp. 475−490 in: *Methods of Soil Analysis*, Part 3 − *Chemical Methods* (D.L. Sparks, A.L. Page, P.A. Helmke, R.H. Loeppert, P.N. Soltanpour, M.A. Tabatabai, C.T. Johnston, and M.E. Sumner, editors). Soil Science Society of America, Madison, Wisconsin, USA.

Tomura, S., Shibasaki, Y., Mizuta, H., and Kitamura, M. (1985) Growth conditions and genesis of spherical and platy kaolinite. *Clays and Clay Minerals*, **33**, 200−206.

Tsuzuki, Y. and Kawabe, I. (1983) Polymorphic transformations of kaolin minerals in aqueous solutions. *Geochimica et Cosmochimica Acta*, **47**, 59−66.

Uehara, G. (2003) Developments in soil chemistry and soil classification. Pp. 67−73 in: *Soil Classification: A Global Desk Reference* (T. Rice, H. Eswaran, B.A. Stewart, and R. Ahrens, editors). CRC Press, Boca Raton, Florida, USA.

Vitousek, P.M. and Sanford, R.L., Jr. (1986) Nutrient cycling in moist tropical forest. *Annual Review of Ecological Systematics*, **17**, 137−167.

Wada, K. and Kakuto, Y. (1983) Intergradient vermiculite-kaolin mineral in a Korean Ultisol. *Clays and Clay Minerals*, **31**, 183−190.

Wada, S. and Mizota, C. (1982) Iron-rich halloysite (10 Å) with crumpled lamellar morphology from Hokkaido, Japan. *Clays and Clay Minerals*, **30**, 315−317.

Watanabe, T., Sawada, Y., Russell, J.D., McHardy, W.J., and Wilson, M.J. (1992) The conversion of montmorillonite to interstratified halloysite-smectite by weathering in the Omi acid clay deposit, Japan. *Clay Minerals*, **27**, 159−173.

Wilson, M.J. (1999) The origin and formation of clay minerals in soils; past, present and future perspectives. *Clay Minerals*, **34**, 7−25.

Yerima, B.P.K., Calhoun, F.G., Senkayi, A.L., and Dixon, J.B. (1985) Occurrence of interstratified kaolinite-smectite in El Salvador Vertisols. *Soil Science Society of America Journal*, **49**, 462−466.

Ziegler, K., Hsieh, J.C.C., Chadwick, O.A., Kelly, E.F., Hendricks, D.M., and Savin, S.M. (2003) Halloysite as a kinetically controlled end product of arid-zone basalt weathering. *Chemical Geology*, **202**, 461−478, doi:10.1016/j.chemgeo.2002.06.001.